Viscous Vortex Dynamics on Surfaces

CUNCHENG ZHU*, University of California San Diego, USA
HANG YIN*, University of California San Diego, USA
ALBERT CHERN, University of California San Diego, USA

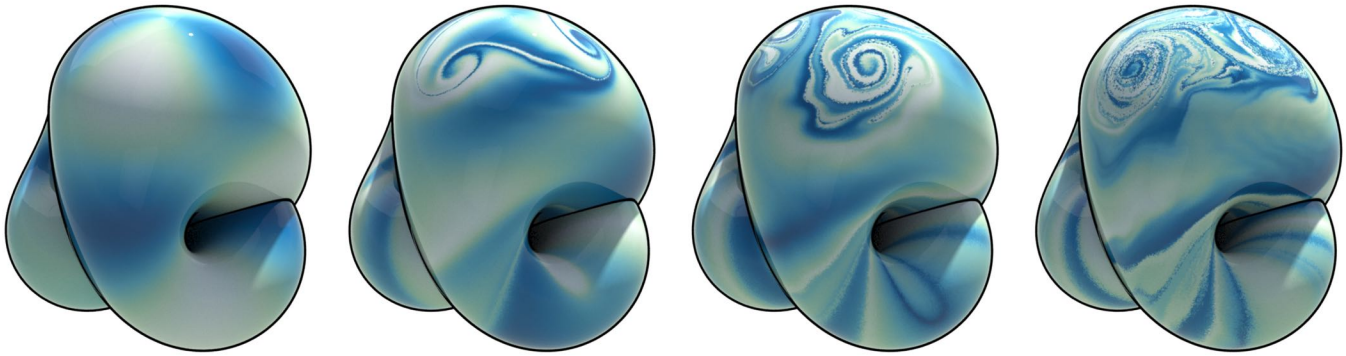

Fig. 1. Simulation of the Navier–Stokes fluid on the non-orientable *Boy surface* using our vorticity method.

We present a vorticity method for simulating incompressible viscous flows on curved surfaces governed by the Navier–Stokes equations. Unlike previous approaches, our formulation incorporates the often-overlooked Gaussian-curvature-dependent term in the viscous force, which influences both the vorticity equation and the evolution of harmonic components. We show that these curvature-related terms are crucial for reproducing physically correct fluid behavior. We introduce an implicit–explicit (IMEX) scheme for solving the resulting system on triangle meshes and demonstrate its effectiveness on surfaces with arbitrary topology, including non-orientable surfaces, and under a variety of boundary conditions. Our theoretical contributions include several explicit formulas: a vorticity jump condition across curvature sheets, a geometric correspondence between friction coefficients and boundary curvature adjustments, and the influence of boundary curvature on harmonic modes. These results not only simplify the algorithmic design but also offer geometric insight into curvature-driven fluid phenomena, such as the emergence of the Kutta condition under free-slip boundaries.

CCS Concepts: • **Computing methodologies** → **Physical simulation**; *Shape analysis*; • **Mathematics of computing** → **Topology**; *Partial differential equations.*

Additional Key Words and Phrases: Fluid simulation, Killing operator, vorticity method, cohomology

*Shared first authors.

Authors' addresses: Cuncheng Zhu, University of California San Diego, 9500 Gilman Dr, MC 0404, La Jolla, CA, 92093, USA, cuzhu@ucsd.edu; Hang Yin, University of California San Diego, 9500 Gilman Dr, MC 0404, La Jolla, CA, 92093, USA, h7yin@ucsd.edu; Albert Chern, University of California San Diego, 9500 Gilman Dr, MC 0404, La Jolla, CA, 92093, USA, alchern@ucsd.edu.

Please use nonacm option or ACM Engage class to enable CC licenses
This work is licensed under a Creative Commons Attribution 4.0 International License.
© 2025 Copyright held by the owner/author(s).
ACM 0730-0301/2025/12-ART178
https://doi.org/10.1145/3763320

ACM Reference Format:
Cuncheng Zhu, Hang Yin, and Albert Chern. 2025. Viscous Vortex Dynamics on Surfaces. *ACM Trans. Graph.* 44, 6, Article 178 (December 2025), 21 pages. https://doi.org/10.1145/3763320

1 INTRODUCTION

Simulating fluid dynamics on curved surfaces has continued to attract attention in computer graphics [Yaeger et al. 1986; Stam 2003; Shi and Yu 2004; Elcott et al. 2007; Azencot et al. 2014; Yang et al. 2019; Huang et al. 2020; Ishida et al. 2020; Cui et al. 2021; Yin et al. 2023; Tao et al. 2024]. Among various formulations of the governing equations, the *vorticity formulation* is particularly attractive [Yaeger et al. 1986; Elcott et al. 2007; Azencot et al. 2014], since vorticity is a scalar quantity that can be advected directly on the surface. In contrast, velocity-based formulations must account for covariant derivatives or parallel transport [Shi and Yu 2004]. However, simulating vorticity on a surface requires additional care. It is only recently that the full vorticity equation for inviscid fluids was explicitly formulated in a way that incorporates nontrivial surface topology [Yin et al. 2023].

In this paper, we derive the vorticity equation for the Navier–Stokes equation on general surfaces M. Even for simply-connected domains, few existing methods in the graphics literature have correctly incorporated the viscous terms. A commonly overlooked detail is that the *Gaussian curvature* K of the surface contributes an additional term to the viscous force in the Navier–Stokes equation. In the vorticity formulation, this leads to the expression:

$$\underbrace{\frac{\partial w}{\partial t} + \mathbf{u} \cdot \nabla w = \nu \Delta w}_{\text{previous model}} + \underbrace{2\nu \operatorname{curl}(K\mathbf{u})}_{\text{curvature term}} \tag{1}$$

where w is the scalar vorticity, $\mathbf{u}$ the velocity field, Δ the Laplace–Beltrami operator, and ν the kinematic viscosity. Furthermore, on non-simply-connected domains, curvature and viscosity also affect the evolution of the *harmonic components* of the velocity field. If $\mathbf{h}$ is

a harmonic vector field and $\mathbf{u}$ is the velocity field, the coefficient $c = \langle\langle \mathbf{h}, \mathbf{u} \rangle\rangle$ evolves according to

$$\underbrace{\frac{dc}{dt} = \iint_M [(\mathbf{h} \times \mathbf{u})w}_{\substack{\text{inviscid part} \\ \text{[Yin et al. 2023]}}} + \underbrace{2\nu(\mathbf{h} \cdot \mathbf{u})K]\, dA + \oint_{\partial M} \nu h_\partial w\, ds,}_{\text{new viscous terms}} \tag{2}$$

where h_∂ denotes the tangential component of $\mathbf{h}$ along the boundary. We show that these geometric terms are essential for capturing physically accurate behavior of viscous flows on curved surfaces, such as the conservation of frictionless rigid body motions.

Our proposed formulation and the accompanying numerical solver apply to general surfaces, including *non-orientable* ones (Figure 1). The framework supports a variety of boundary conditions, including the commonly used *no-slip*, *Navier friction*, and *free-slip* boundary conditions.

We highlight several additional findings:

- We analyze the effect of curvature term in (1) and show that a *curvature sheet* can maintain a *jump discontinuity* in vorticity, even in the presence of the diffusion term $\nu\Delta w$. We derive an explicit formula for this jump condition (Theorem 2.3).
- We discover a geometric equivalence: setting the friction coefficient is effectively equivalent to modifying the *geodesic curvature* of the boundary. Based on this principle, imposing boundary friction corresponds to adjusting the boundary's intrinsic angles (Sections 3.2 and 5.3.1).
- We introduce the concept of combining Gaussian curvature and the boundary geodesic curvature into a unified *Gauss–Bonnet curvature density*. This reveals that the boundary curvature affects vorticity and harmonic components in the same way as Gaussian curvature. Notably, the curvature terms in (1) and (2) remain important even on flat domains with curved boundaries (Section 3.1). This insight also enables an elegant and stable discretization for incorporating vortex phenomena at the boundary.
- This curvature effect *directly gives rise to the Kutta condition*—a classical result in aerodynamics stating that flow must detach cleanly at the sharp trailing edge of an airfoil. Traditionally, this behavior is attributed to frictional boundary layers. However, we demonsrate that our formulation reproduces the Kutta condition naturally under *frictionless free-slip boundaries* without explicitly modeling boundary layers (Remark 3.1, Figure 5).

1.1 Previous Work

There has been a long history of developing fluid simulation methods on curved surfaces in computer graphics.

1.1.1 Fluid Simulation on the Sphere. A number of works have focused specifically on fluid simulation on the sphere. Yaeger et al. [1986] introduced a vorticity formulation for this setting. However, their formulation omitted the curvature-related term in (1), instead modeling the voticity dynamics with the convection-diffusion equation $\frac{\partial w}{\partial t} + \mathbf{u} \cdot \nabla w = \nu\Delta w$. Hill and Henderson [2016] derived the fluid equations more carefully in spherical coordinates using a velocity-based formulation and noted that several prior works neglected geometric terms, though their discussion is primarily limited to the inviscid case. Huang et al. [2020] presented a chemomechanical simulation on the sphere using a velocity-based formulation. Their method implicitly includes a proper viscous force by taking the divergence of the total stress, but the formulation is written in spherical coordinates and does not generalize directly to arbitrary surfaces.

1.1.2 Fluid Simulation on General Surfaces. Stam [2003] extended fluid simulation to general surfaces using a velocity-based formulation in local coordinates. In this approach, viscosity is modeled by applying the Laplace–Beltrami operator directly to each coordinate component of the velocity. Carvalho et al. [2012] noted this treatment is a simplication, pointing out that on curved surfaces, the divergence of the strain rate cannot generally be reduced to a componentwise Laplacian.

Hegeman et al. [2009] and Padilla [2018] proposed simulating fluid flow by first conformally mapping the surface to a round sphere and solving an effective system on the sphere. However, these methods apply only to topological spheres and do not include viscosity.

More general approaches rely on coordinate-free calculus applied directly to discrete surfaces. Shi and Yu [2004] described the inviscid Euler equation on surfaces using parallel transport for velocity vectors. Elcott et al. [2007] and Azencot et al. [2014] formulated the vorticity–streamfunction method for simplicial meshes, but their vorticity equation also takes the form $\frac{\partial w}{\partial t} + \mathbf{u} \cdot \nabla w = \nu\Delta w$, following [Yaeger et al. 1986] and omitting the curvature term. Cui et al. [2021] applied a spectral method for the velocity-based formulation on surfaces, while Tao et al. [2024] used a particle-in-mesh hybrid method for the vorticity equation on surfaces. Both works similarly exclude the curvature term in their modeling of viscosity.

Curved-surface fluid simulations have also been studied in the Computational Fluid Dynamics (CFD) community. Nitschke et al. [Nitschke et al. 2017] used Discrete Exterior Calculus (DEC) (also used in [Elcott et al. 2007]) with a velocity-based formulation that includes a correct viscous term. Gross et al. [2020] developed an exterior calculus framework for meshless discretization of a streamfunction-based method on surfaces. Their focus is limited to topological spheres, and they note that modeling the dynamics of harmonic components on non-simply-connected domains remains an open problem. Nitschke et al. [2021] similarly observed that vorticity–streamfunction methods (including [Elcott et al. 2007] and [Azencot et al. 2014]) are not well-suited for non-simply-connected domains due to the absence of a model for harmonic field dynamics.

Vanneste [2021] simulated the vorticity–streamfunction system on a non-orientable Möbius strip. In that setting, the harmonic component is updated by tracking circulation along the boundary. However, the method does not generalize to harmonic components arising from genus. A small dissipation term of the form $\frac{\partial w}{\partial t} + \mathbf{u} \cdot \nabla w = \nu\Delta w$ is added to the vorticity equation, with the author noting that it does not represent the true viscous force since it omits the curvature-related term.

Yin et al. [2023] derived and incorporated the correct dynamics for harmonic components in the inviscid vorticity–streamfunction framework of [Azencot et al. 2014], but their work focuses primarily on the inviscid Euler fluids.

To the best of our knowledge, our algorithm is the first to incorporate both the correct viscous terms and the general harmonic field dynamics on surfaces of arbitrary topology—including non-orientable surfaces.

1.1.3 Theoretical Foundations. Formulations of the Navier–Stokes equations on manifolds date back to Ebin and Marsden [1970], though the viscous term was not expressed using the proper Laplacian. [Taylor et al. 1996, page 600, Chapter 17.5] presents the correct formulation of the viscous force, invoking the *Weitzenböck formula* to relate various Laplacians. The proper viscous modeling on Riemannian manifolds is further emphasized in more recent work by [Chan et al. 2017] and [Samavaki and Tuomela 2020].

1.2 Overview

We present a detailed derivation of the Navier–Stokes equation on surfaces and its vorticity formulation in Section 2. The derivation of the boundary conditions and the extension to non-orientable surfaces are given in Section 3 and Section 4 respectively. Our numerical algorithm is described in Section 5, followed by simulation results in Section 6.

2 EQUATIONS OF MOTION

The goal of this section is to derive the vorticity formulation of the Navier–Stokes equation on surfaces. In Sections 2.1 and 2.2, we clarified the appropriate form of the Navier–Stokes equation for surfaces. We then derive the corresponding vorticity equation, along with the accompanying harmonic field equation, in Section 2.3.

Let the fluid domain M be a two-dimensional Riemannian manifold. Here we assume that M is oriented while leaving the discussion of non-orientable domains to Section 4.

Let $\mathfrak{X} \coloneqq \Gamma(TM)$ denote the space of tangent vector fields. Define the subspace $\mathfrak{X}_{\text{div}} \subset \mathfrak{X}$ as the collection of divergence-free vector fields with no-penetration boundary condition:

$$\mathfrak{X}_{\text{div}} \coloneqq \{\mathbf{v} \in \mathfrak{X} \mid \operatorname{div} \mathbf{v} = 0 \text{ in } M, \langle \mathbf{v}, \mathbf{n} \rangle = 0 \text{ on } \partial M\}. \tag{3}$$

The space $\mathfrak{X}_{\text{div}}$ is the feasible space for the velocity field of an incompressible flow on M. Here, $\mathbf{n}$ is the unit vector at ∂M that is tangent to M and inward normal to ∂M.

At each time t, the fluid velocity is a vector field $\mathbf{u}_t \in \mathfrak{X}_{\text{div}}$. We will suppress the subscript t for these time dependent variables.

2.1 Incompressible Navier–Stokes Equation

The *incompressible Navier–Stokes equation* is given by

$$\frac{\partial}{\partial t}\mathbf{u} + \nabla_{\mathbf{u}}\mathbf{u} = -\operatorname{grad} p + \operatorname{div} \boldsymbol{\tau} \tag{4}$$

where p is a scalar function representing the pressure or the Lagrange multiplier that keeps $\mathbf{u}$ in the subspace $\mathfrak{X}_{\text{div}}$, and $\boldsymbol{\tau} \in \Gamma(\odot^2 TM)$ is a symmetric bivector (two-vector) tensor representing viscous stress.[1] Here, ∇ is the covariant derivative (a.k.a. the Levi-Civita connection) for the tangent bundle.

[1]The notation $\odot$ for the tensor bundle $\odot^2 TM = TM \odot TM$ is the symmetric tensor product. In particular, $\odot^2 TM \subset \otimes^2 TM$ is the bundle for symmetric tensors of bivector type.

The divergence $(\operatorname{div} \boldsymbol{\tau})$ of a symmetric bivector $\boldsymbol{\tau}$ also depends on the Levi-Civita connection. It represents the net force arising from the stress $\boldsymbol{\tau}$. In coordinate index notation, $(\operatorname{div} \boldsymbol{\tau})^i = \nabla_j \tau^{ij}$.

To close the system (4), one must model how the viscous stress tensor $\boldsymbol{\tau}$ depends on the variable $\mathbf{u}$. For Newtonian fluids, the viscous stress tensor $\boldsymbol{\tau}$ is a linear function of the velocity gradient $\nabla\mathbf{u}$ in a particular form. Within the tensor $\nabla\mathbf{u}$ there is a component that quantifies the rate of shearing or non-isometric deformations the flow experiences. This quantity is called the *strain rate*. The viscous stress tensor is modeled to be proportional to this quantity. This model will be stated in Section 2.1.2.

2.1.1 Strain Rate. The *symmetric part* of the velocity gradient corresponds to the rate of non-isometric deformation. This symmetrized gradient has a natural geometric definition, given as follows:

Definition 2.1 (Killing operator)**.** *Let $g \in \Gamma(\odot^2 T^*M)$ denote the metric tensor on M. The **Killing operator** is the differential operator $\mathcal{K}\colon \Gamma(TM) \to \Gamma(\odot^2 T^*M)$ acting on vector fields, defined as half the Lie derivative of the metric tensor along the vector field:*

$$\mathcal{K}\mathbf{u} \coloneqq \frac{1}{2}\mathscr{L}_{\mathbf{u}}\, g. \tag{5}$$

We now expand the definition of the Lie derivative. For a velocity field $\mathbf{u}$, the tensor $\mathscr{L}_{\mathbf{u}}\, g$ represents the rate of change of the pullback metric under the flow generated by $\mathbf{u}$. Explicitly, $\mathscr{L}_{\mathbf{u}}\, g = \frac{\partial}{\partial t}|_{t=0}(\varphi_t{}^* g)$, where φ_t is the flow map generated by $\mathbf{u}$. In other words, $\mathcal{K}\mathbf{u}$ directly measures the rate of non-isometric deformation induced by the flow of $\mathbf{u}$.

The following proposition shows that the strain rate $\mathcal{K}\mathbf{u}$ indeed recovers the symmetrized velocity gradient.

Proposition 2.1. *The symmetric bilinear form $\mathcal{K}\mathbf{u} \in \Gamma(\odot^2 T^*M)$ for a vector field $\mathbf{u} \in \Gamma(TM)$ can be explicitly expressed as follows. At each point $p \in M$, for all $\mathbf{a}, \mathbf{b} \in T_pM$:*

$$(\mathcal{K}\mathbf{u})[\![\mathbf{a}, \mathbf{b}]\!] = \frac{1}{2}\left(\langle \nabla_{\mathbf{a}}\mathbf{u}, \mathbf{b}\rangle + \langle \nabla_{\mathbf{b}}\mathbf{u}, \mathbf{a}\rangle\right). \tag{6}$$

Proof. Appendix A.1. □

Remark 2.1. *In an orthonormal basis, equation (6) shows that $\mathcal{K}\mathbf{u}$ corresponds to the 2-by-2 matrix $\mathcal{K}\mathbf{u} = \frac{1}{2}(\nabla\mathbf{u} + (\nabla\mathbf{u})^\intercal)$. That is, $\mathcal{K}\mathbf{u}$ is the symmetric part of the matrix $\nabla\mathbf{u}$, familiar to readers with a continuum mechanics background. However, the expression $(\nabla\mathbf{u} + \nabla\mathbf{u}^\intercal)$ informally combines tensors of different types: $\nabla\mathbf{u}$ sends vectors to vectors, while $\nabla\mathbf{u}^\intercal$ sends covectors to covectors. Writing $(\nabla\mathbf{u} + \nabla\mathbf{u}^\intercal)$ precisely requires an additional layer of metric conversions. For clarity, we will therefore continue working with the invariant object $\mathcal{K}\mathbf{u}$.*

Definition 2.2 (Killing vector field)**.** *A vector field $\mathbf{v}$ is called a **Killing vector field** if $\mathcal{K}\mathbf{v} = 0$.*

Killing vector fields generate isometric flows—rigid motions that do not involve shearing. Domains with continuous symmetries, such as surfaces of revolution, admit Killing vector fields. If the fluid velocity is a Killing field, then the fluid experiences no internal viscous stress.

2.1.2 Constitutive Model. The viscous stress in (4) is proportional to the strain rate

$$\boldsymbol{\tau} = 2\nu(\mathcal{K}\mathbf{u})^\sharp. \tag{7}$$

where $\nu \geq 0$ is the kinematic viscosity coefficient. Here, the $\sharp$ operator in $(\mathcal{K}\mathbf{u})^\sharp$ denotes the isomorphism $\odot^2 T^*M \to \odot^2 TM$ with respect to the Frobenius norm for order-2 tensors. In index notation, $\tau^{ij} = 2\nu g^{ik} g^{j\ell} (\mathcal{K}\mathbf{u})_{k\ell}$.

The stress–strain relationship (7) can also be derived from variational principles via the *Rayleigh dissipation functional*:

$$\mathcal{R} \colon \mathfrak{X}_{\mathrm{div}} \to \mathbb{R}, \quad \mathcal{R}[\mathbf{u}] \coloneqq \iint_M \nu |\mathcal{K}\mathbf{u}|^2 \, dA, \tag{8}$$

where $|\cdot|^2$ is the Frobenius norm. The dissipation functional (8) quantifies the rate of energy dissipation, modeled under the physical assumption that the dissipation depends quadratically and isotropically on the strain rate. The viscous force in the momentum equation (4) is then obtained via Rayleigh's variational principle: the viscous force is the negative gradient of the Rayleigh dissipation functional, added directly to the inviscid equation of motion (the Euler equation).

We recall the notion of a functional gradient:

Definition 2.3. *The gradient of a functional $\mathcal{F} \colon \mathfrak{X}_{\mathrm{div}} \to \mathbb{R}$ at $\mathbf{u} \in \mathfrak{X}_{\mathrm{div}}$, with respect to the L^2 inner product structure $\langle\!\langle \cdot, \cdot \rangle\!\rangle \coloneqq \iint_M \langle \cdot, \cdot \rangle \, dA$ on $\mathfrak{X}_{\mathrm{div}}$, is the vector field $(\operatorname{grad} \mathcal{F})|_{\mathbf{u}} \in \mathfrak{X}_{\mathrm{div}}$ satisfying*

$$\left. \frac{d}{d\epsilon} \right|_{\epsilon=0} \mathcal{F}[\mathbf{u} + \epsilon \mathring{\mathbf{u}}] = \langle\!\langle \operatorname{grad} \mathcal{F}|_{\mathbf{u}}, \mathring{\mathbf{u}} \rangle\!\rangle \tag{9}$$

for any variation $\mathring{\mathbf{u}} \in \mathfrak{X}_{\mathrm{div}}$ that vanishes on ∂M.

Proposition 2.2. *The functional gradient $(\operatorname{grad} \mathcal{R})$ of $\mathcal{R}$ defined in (8) is given by*

$$(\operatorname{grad} \mathcal{R})|_{\mathbf{u}} = -2\nu \operatorname{div}(\mathcal{K}\mathbf{u})^\sharp. \tag{10}$$

Proof. Appendix A.4. □

2.1.3 Summary. The Navier Stokes equation (4) with the stress–strain relation (7) becomes:

$$\boxed{\frac{\partial}{\partial t}\mathbf{u} + \nabla_{\mathbf{u}}\mathbf{u} = -\operatorname{grad} p + 2\nu \operatorname{div}(\mathcal{K}\mathbf{u})^\sharp.} \tag{11}$$

This equation can be viewed as the Euler equation $\frac{\partial}{\partial t}\mathbf{u} + \nabla_{\mathbf{u}}\mathbf{u} = -\operatorname{grad} p$, augmented by the additional gradient descent term $-(\operatorname{grad} \mathcal{R})|_{\mathbf{u}}$ of the dissipation functional $\mathcal{R}$.

2.2 Hodge, Bochner, and Viscous Laplacians

On a flat Euclidean domain, the divergence of the symmetrized gradient equals the vector Laplacian when applied to divergence-free fields, $\nabla \cdot (\nabla \mathbf{u} + \nabla \mathbf{u}^\intercal) = \Delta \mathbf{u} + \nabla(\nabla \cdot \mathbf{u}) = \Delta \mathbf{u}$, which leads to the familiar form of the Navier–Stokes equation $\frac{\partial}{\partial t}\mathbf{u} + \nabla_{\mathbf{u}}\mathbf{u} = -\operatorname{grad} p + \nu \Delta \mathbf{u}$. However, this vector identity *does not* hold when the domain has curvature.

There are *three* relevant surface Laplacians for vector fields in this context, each defined via the functional gradient of a Dirichlet-type energy.

2.2.1 Dirichlet Energies.

Definition 2.4 (Standard Dirichlet energy)**.** *The **standard Dirichlet energy** for a vector field $\mathbf{v} \in \Gamma(TM)$ is:*

$$\mathcal{E}_{\mathrm{D}}[\mathbf{v}] \coloneqq \frac{1}{2} \iint_M |\nabla \mathbf{v}|^2 \, dA. \tag{12}$$

Definition 2.5 (Hodge-Dirichlet energy)**.** *The **Hodge-Dirichlet energy** for a vector field $\mathbf{v} \in \Gamma(TM)$ is:*

$$\mathcal{E}_{\mathrm{H}}[\mathbf{v}] \coloneqq \frac{1}{2} \iint_M (|d\mathbf{v}^\flat|^2 + |\delta \mathbf{v}^\flat|^2) \, dA, \tag{13}$$

where d and δ denote the exterior derivative and the codifferential respectively.

Note that if $\mathbf{v}$ is restricted to $\mathfrak{X}_{\mathrm{div}}$ (divergence-free fields, where $\mathbf{v}^\flat$ is coclosed), the Hodge-Dirichlet energy simplifies to

$$\mathcal{E}_{\mathrm{H}}[\mathbf{v}] = \frac{1}{2} \iint_M |d\mathbf{v}^\flat|^2 \, dA, \quad \mathbf{v} \in \mathfrak{X}_{\mathrm{div}}. \tag{14}$$

Here, $d\mathbf{v}^\flat$ is the vorticity 2-form, corresponding to the *skew-symmetric part* of $2\nabla \mathbf{v}$.

Definition 2.6 (Viscous-Dirichlet energy)**.** *The **viscous-Dirichlet energy**—also called the **Killing energy** [Ben-Chen et al. 2010]—for a vector field $\mathbf{v} \in \Gamma(TM)$ is:*

$$\mathcal{E}_{\mathrm{V}}[\mathbf{v}] \coloneqq \iint_M |\mathcal{K}\mathbf{v}|^2 \, dA. \tag{15}$$

The standard Dirichlet energy measures the smoothness of the vector field, a notion commonly used in vector field design in geometry processing. The Hodge-Dirichlet energy, when restricted to divergence-free fields, measures the L^2-strength of the vorticity. The viscous-Dirichlet energy measures the rate of energy dissipation ($\mathcal{R} = \nu \mathcal{E}_{\mathrm{V}}$; see (8)) and also quantifies the deviation of a vector field from being a Killing field.

Remark 2.2. *When M is a flat Euclidean domain (ignoring boundary effects), the three Dirichlet energies are equal. In fluid mechanics, they are all referred to as the **enstrophy** of the flow, with physical interpretations relating to both the vorticity magnitude and the level of dissipation. However, to our knowledge, there is no universal agreed-upon definition of enstrophy for fluid on a Riemannian manifold, where these two interpretations diverge.*

2.2.2 Vector Laplacians. The following are the three vector Laplacians associated with the three Dirichlet energies.

Definition 2.7. *The **Bochner Laplacian** (or **connection Laplacian**) for a vector field $\mathbf{v} \in \Gamma(TM)$ is defined by*

$$\Delta_{\mathrm{B}} \mathbf{v} \coloneqq -(\operatorname{grad} \mathcal{E}_{\mathrm{D}})|_{\mathbf{v}}. \tag{16}$$

The Bochner Laplacian satisfies $\Delta_{\mathrm{B}} \mathbf{v} = \operatorname{div}(\nabla \mathbf{v})$ where div denotes the connection divergence (the negative L^2-adjoint of ∇). An alternative expression is $\Delta_{\mathrm{B}} \mathbf{v} = \star^{-1} d^\nabla \star \nabla \mathbf{v}$ where $\mathbf{v}$ is regarded as a vector-valued 0-form, and d^∇ is the covariant exterior derivative for vector-valued k-forms.

Definition 2.8. *The **Hodge Laplacian** for a vector field $\mathbf{v} \in \Gamma(TM)$ is defined by*

$$\Delta_{\mathrm{H}} \mathbf{v} \coloneqq -(\operatorname{grad} \mathcal{E}_{\mathrm{H}})|_{\mathbf{v}}. \tag{17}$$

The Hodge Laplacian takes the familiar form: $\Delta_H \mathbf{v} = -((d\delta + \delta d)\mathbf{v}^\flat)^\sharp$, standard in exterior calculus.

Definition 2.9. *The **viscous Laplacian** for a vector field $\mathbf{v} \in \Gamma(TM)$ is defined by*

$$\Delta_V \mathbf{v} \coloneqq -(\operatorname{grad} \mathcal{E}_V)|_{\mathbf{v}}. \tag{18}$$

The viscous Laplacian is given by $\Delta_V \mathbf{v} = 2 \operatorname{div}(\mathcal{K}\mathbf{v})^\sharp$, where $\operatorname{div} \circ \sharp$ is the negative adjoint of $\mathcal{K}$.

All three Laplacians are self-adjoint (with respect to L^2) and are negative semi-definite elliptic operators. Their differences become apparent when examining their kernels (zero eigenspaces). For simplicity, we restrict $\mathbf{v} \in \mathfrak{X}_{\text{div}}$.

- $\Delta_B \mathbf{v} = \mathbf{0}$ if and only if $\mathbf{v} \in \mathfrak{X}_{\text{div}}$ is *parallel*. In particular, Δ_B has a nontrivial kernel only when the domain is flat.
- $\Delta_H \mathbf{v} = \mathbf{0}$ if and only if $\mathbf{v} \in \mathfrak{X}_{\text{div}}$ is *harmonic*. Thus, Δ_H has a kernel if and only if the domain is not simply connected.
- $\Delta_V \mathbf{v} = \mathbf{0}$ if and only if $\mathbf{v} \in \mathfrak{X}_{\text{div}}$ is a *Killing field*. Consequently, Δ_V has a kernel if and only if the metric domain admits continuous symmetries.

The kernel of Δ_B are parallel translational flows, which exist only in Euclidean whose boundaries (if any) are straight and compatible with translation, such as in a pipe domain. In contrast, the existence of a kernel for Δ_H depends solely on the topology of the domain. Meanwhile, the existence of a kernel for Δ_V reflects the presence of domain symmetries. For example, Killing fields exist on simply connected curved domains such as the round sphere.

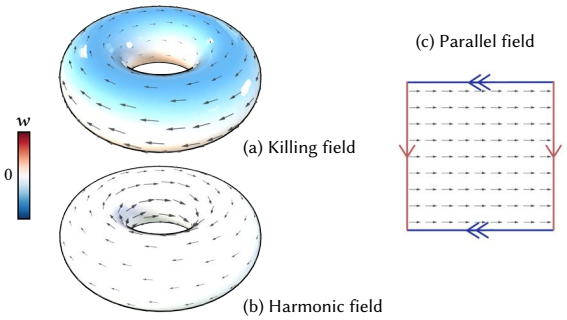

Fig. 2. Kernels of the Laplacians Δ_V, Δ_H, and Δ_B on tori. (a) A vector field in $\ker(\Delta_V)$ is a Killing field, which generally has nonzero vorticity. (b) A vector field in $\ker(\Delta_H)$ is harmonic and therefore has zero vorticity. (c) A vector field in $\ker(\Delta_B)$ is parallel, which is possible on a flat torus; on this domain Δ_B, Δ_H, Δ_V share the same kernel.

The following theorem states the precise relationship between the three Laplacians.

Theorem 2.1 (Weitzenböck identity)**.** *When applied to divergence-free vector fields $\mathbf{v} \in \mathfrak{X}_{\text{div}}$ on a surface, the Bochner, Hodge, and viscous Laplacians are related by:*

$$\Delta_B \mathbf{v} = \Delta_H \mathbf{v} + K\mathbf{v} = \Delta_V \mathbf{v} - K\mathbf{v}, \quad \mathbf{v} \in \mathfrak{X}_{\text{div}}, \tag{19}$$

where K is the Gaussian curvature of the surface.

Proof. Appendix A.6. □

2.2.3 Summary. The Navier–Stokes equation can be written in terms of the different Laplacians as any of the following equivalent forms:

$$\boxed{\frac{\partial}{\partial t}\mathbf{u} + \nabla_{\mathbf{u}}\mathbf{u} = -\operatorname{grad} p + \nu \Delta_V \mathbf{u}} \tag{20}$$

$$\boxed{\frac{\partial}{\partial t}\mathbf{u} + \nabla_{\mathbf{u}}\mathbf{u} = -\operatorname{grad} p + \nu \Delta_B \mathbf{u} + \nu K\mathbf{u}} \tag{21}$$

$$\boxed{\frac{\partial}{\partial t}\mathbf{u} + \nabla_{\mathbf{u}}\mathbf{u} = -\operatorname{grad} p + \nu \Delta_H \mathbf{u} + 2\nu K\mathbf{u}.} \tag{22}$$

A direct consequence of the Navier–Stokes equation is that if a Killing field exists, the component of the velocity field along the Killing field is conserved.

Theorem 2.2. *Suppose $\mathbf{v} \in \mathfrak{X}_{\text{div}}$ is a Killing field, and let $\mathbf{u}$ be a solution to the Navier–Stokes equation. Then $\langle\!\langle \mathbf{u}, \mathbf{v} \rangle\!\rangle$ remains constant in time.*

Proof. Appendix A.2. □

2.3 Vorticity Formulation

We now derive the vorticity formulation of the Navier–Stokes equation.

2.3.1 Vorticity Equation. Applying the $\flat$ operator to (22), we obtain the Navier–Stokes equation in covector form:

$$\frac{\partial}{\partial t}\mathbf{u}^\flat + \mathcal{L}_{\mathbf{u}}\,\mathbf{u}^\flat = -d\left(p - \frac{1}{2}|\mathbf{u}|^2\right) - \nu \delta d \mathbf{u}^\flat + 2\nu K \mathbf{u}^\flat. \tag{23}$$

Taking the exterior derivative of (23), and letting

$$\omega \coloneqq d\mathbf{u}^\flat \in \Omega^2(M) \tag{24}$$

denote the vorticity 2-form, we obtain:

$$\frac{\partial}{\partial t}\omega + \mathcal{L}_{\mathbf{u}}\,\omega = -\nu d\delta\omega + 2\nu d(K\mathbf{u}^\flat). \tag{25}$$

Let the vorticity scalar function be defined by

$$w = \star^{-1}\omega \in \Omega^0(M). \tag{26}$$

Then (25) becomes

$$\frac{\partial}{\partial t}w + \mathcal{L}_{\mathbf{u}}\,w = \nu \Delta w + 2\nu \star^{-1} d(K\mathbf{u}^\flat), \tag{27}$$

where $\Delta = \star^{-1} d \star d$ is the standard (negative semi-definite) Laplace–Beltrami operator for scalar functions.

In vector calculus notation, this reads:

$$\boxed{\frac{\partial}{\partial t}w + \mathbf{u} \cdot \nabla w = \nu \Delta w + 2\nu \operatorname{curl}(K\mathbf{u}).} \tag{28}$$

Here, in two dimensions, we use the scalar curl operator $\operatorname{curl} \coloneqq -\operatorname{div} \circ J$, where J denotes the 90° rotation operator.

Remark 2.3 (Effect of curvature on vorticity)**.** *Equations* (25) *and* (28) *show that the vorticity evolves via a convection-diffusion process with an additional curvature-driven term $2\nu d(K\mathbf{u}^\flat)$. Applying the Leibniz rule $d(K\mathbf{u}^\flat) = dK \wedge \mathbf{u}^\flat + K d\mathbf{u}^\flat$ we can expand the curvature term $2\nu \operatorname{curl}(K\mathbf{u})$ as:*

$$2\nu \operatorname{curl}(K\mathbf{u}) = 2\nu \langle -J\mathbf{u}, \operatorname{grad} K \rangle + 2\nu K w. \tag{29}$$

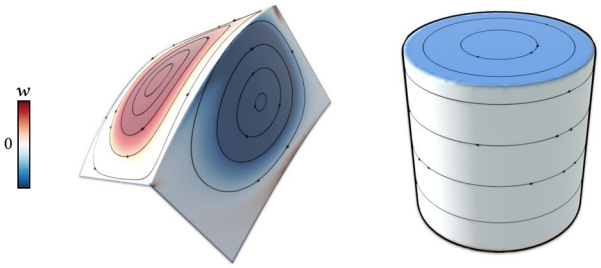

Fig. 3. A singular sheet in the Gaussian curvature gives rise to a jump discontinuity in the vorticity, shown by the color (*cf.* Theorem 2.3). Left: Vorticity distribution in a simulation on a surface with a curved ridge. Right: The rigid body rotation field on a cylinder exhibits a vorticity jump that agrees with Theorem 2.3.

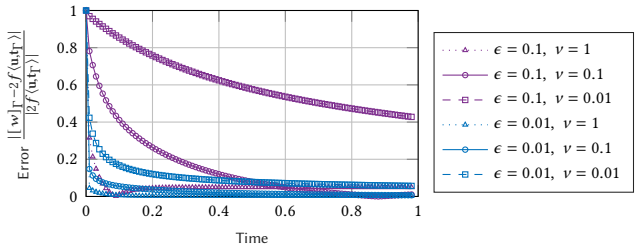

Fig. 4. Validation of (30) with various viscosity ν on a cylinder of radius $R = 1/2$ (Figure 3, right) triangulated with averaged edge length ϵ. The Gaussian curvature in its regular and singular parts is given by $K = 0 + \frac{1}{R}\delta_\Gamma$ (*i.e.* $f = 2$ in (30)) where Γ is the rim of the cylinder, and the Dirac δ is smoothed with thickness $O(\epsilon)$. As $\epsilon \to 0$, the relative error of (30) rapidly reduces over time for all ν.

These terms can induce a vorticity confinement effect, opposing the diffusion $\nu\Delta w$, and can lead to soliton-like behavior in the vorticity field.

To best illustrate this effect, consider the case where Gaussian curvature is concentrated along a curve segment $\Gamma \subset M$. Specifically, take $K = K_{\text{reg}} + f\delta_\Gamma$, where K_{reg} is a smooth function (the regular part of the curvature), and δ_Γ is the Dirac δ-distribution supported on Γ (a singular curvature sheet). The factor f is a smooth function defined along Γ. More precisely, for any test function $\varphi\colon M \to \mathbb{R}$, $\int_M K\varphi\, dA = \int_\Omega K_{\text{reg}}\varphi\, dA + \int_\Gamma f\varphi\, ds$. In this setting, the vorticity develops a jump discontinuity across Γ characterized by the following jump condition (see also Figure 3):

Theorem 2.3 (Curvature sheet and vorticity jump)**.** *Under the vorticity equation* (28) *with $K = K_{\text{reg}} + f\delta_\Gamma$ and any $\nu > 0$, the vorticity w satisfies the jump condition*

$$[w]_\Gamma = 2f\langle \mathbf{u}, \mathbf{t}_\Gamma\rangle \tag{30}$$

where $\mathbf{t}_\Gamma$ is the tangent vector of Γ and $[w]_\Gamma$ denotes the jump of w across Γ in the direction $J\mathbf{t}_\Gamma$ normal to Γ. Specifically, for each $x \in \Gamma$, $[w]_\Gamma(x) = \lim_{\epsilon \searrow 0^+} w(\gamma(\epsilon)) - w(\gamma(-\epsilon))$, where $\gamma\colon (-a, a) \to M$ is any smooth curve with $\gamma(0) = x$ and $\gamma'(0) = J\mathbf{t}$.

Proof. Appendix B.1 □

Remark 2.4. *The jump condition* (30) *is independent of the viscosity ν. This naturally leads to the question of whether, in the limit $\nu \to 0$, the jump vanishes abruptly or continuously? To analyze this limiting behavior, we regularize the curvature singularity by smoothing the curvature sheet with thickness ϵ. We now consider the limiting process involving both parameters ϵ and ν (see Figure 4 for a numerical example). For nonzero ϵ and ν, there exists a relaxation time τ for* (30) *to emerge after the initial condition. Dimension analysis shows that $\tau = O(\epsilon^2/\nu)$.*[2] *If $\epsilon^2 \to 0$ faster than $\nu \to 0$, the jump condition emerges, and the resulting jump is independent of the value of ν. In contrast, if $\epsilon > 0$ is fixed while $\nu \to 0$, then the jump vanishes smoothly. The condition* (30) *is to be interpreted under the assumption $\epsilon = 0$, in which case the jump is independent of ν. In practice, discretization introduces a finite $\epsilon \approx$ edge length, and thus both parameters play a role in numerical results (Figure 4).*

[2]By Buckingham's Π theorem, three variables τ, ϵ, ν, which involve only the dimensions of length and time, must be related through a dimensionless constant. In this case, the relation is $\nu\tau/\epsilon^2 = C$.

2.3.2 Velocity Reconstruction. To complete (28), we describe how $\mathbf{u}$ is reconstructed from the variable w. This is achieved using a streamfunction and, when the domain is non-simply-connected, harmonic fields. This standard procedure is also detailed in [Yin et al. 2023, § 2.3–2.6 and § B] and [Azencot et al. 2014, Eq. (1)].

Definition 2.10. *Let $\mathfrak{H} \coloneqq \{\mathbf{h} \in \mathfrak{X}_{\text{div}} \mid d\mathbf{h}^\flat = 0\} \subset \mathfrak{X}_{\text{div}}$ be the space of **harmonic vector fields**. Let $m \coloneqq \dim(\mathfrak{H})$.*

These harmonic vector fields are divergence-free and curl-free with the no-penetration boundary condition. The corresponding 1-forms $\mathcal{H}^1_C \coloneqq \mathfrak{H}^\flat$ are harmonic 1-forms satisfying the co-Dirichlet (Neumann) boundary condition: $d\mathbf{h}^\flat = 0, d \star \mathbf{h}^\flat = 0, j^* \star \mathbf{h}^\flat = 0$, where $j\colon \partial M \hookrightarrow M$ is the inclusion map of the boundary. The dimension m of $\mathfrak{H}$ is finite and equals the first Betti number of M, *i.e.* the dimension of its first homology group.

Let $\mathbf{h}_1, \ldots, \mathbf{h}_m$ be a time-independent, L^2-orthonormal basis for $\mathfrak{H}$. By the Hodge–Morrey–Friedrichs decomposition, any $\mathbf{u} \in \mathfrak{X}_{\text{div}}$ can be expressed as

$$\mathbf{u} = -J \operatorname{grad} \psi + \sum_{i=1}^{m} c_i \mathbf{h}_i, \quad (\text{or } \mathbf{u}^\flat = \star^{-1} d\psi + \textstyle\sum_{i=1}^m c_i \mathbf{h}_i^\flat), \tag{31}$$

where the *streamfunction* $\psi \in \Omega^0(M)$ is a scalar function satisfying a zero-Dirichlet boundary condition[3] $\psi|_{\partial M} = 0$, and $c_i \in \mathbb{R}$ are time-dependent coefficients whose evolution will be discussed in Section 2.3.3.

The streamfunction ψ is uniquely determined (up to an additive constant if $\partial M = \varnothing$) by the vorticity via the Poisson problem:

$$\begin{cases} -\Delta\psi = w & \text{in } M \\ \psi = 0 & \text{on } \partial M. \end{cases} \tag{32}$$

[3]In the literature of 2D streamfunction representation, the streamfunctions are often described as having constant Dirichlet boundary conditions, with different constants for each connected component of the boundary. These cases are handled by the harmonic part $\sum_{i=1}^m c_i \mathbf{h}_i$.

2.3.3 Evolution of the Harmonic Part. The coefficients c_i in (31) evolve over time [Yin et al. 2023]. The dynamics of c_i is nontrivial even in the inviscid case, derived in [Yin et al. 2023, §3]. In sum, the inviscid evolution of c_i is given by $\frac{dc_i}{dt} = \iint_M (\mathbf{h}_i \times \mathbf{u}) w \, dA$, which is obtained by taking the L^2 product of the Euler equation in *Lamb's form* $\frac{\partial}{\partial t}\mathbf{u}^\flat = -i_{\mathbf{u}}\omega - d(p + \frac{1}{2}|\mathbf{u}|^2)$ [Yin et al. 2023, Eq. (23)] with the harmonic basis $\mathbf{h}_i$. Here, Lamb's Euler equation is obtained by expanding Cartan's formula $\mathscr{L}_{\mathbf{u}}\,\mathbf{u}^\flat = i_{\mathbf{u}} d\mathbf{u}^\flat + d i_{\mathbf{u}}\mathbf{u}^\flat = i_{\mathbf{u}}\omega + d|\mathbf{u}|^2$, where $i_{\mathbf{u}}$ is the interior product.

Now, we derive the viscous case in a similar fashion.

First, we rewrite (23) in Lamb's form:

$$\frac{\partial}{\partial t}\mathbf{u}^\flat = -i_{\mathbf{u}}\omega - d\left(p + \tfrac{1}{2}|\mathbf{u}|^2\right) - \nu\delta\omega + 2\nu K\mathbf{u}^\flat. \tag{33}$$

To derive the equation for $c_i = \langle\!\langle \mathbf{u}, \mathbf{h}_i \rangle\!\rangle = \langle\!\langle \mathbf{u}^\flat, \mathbf{h}_i^\flat \rangle\!\rangle$, we take the L^2 product between (33) and $\mathbf{h}_i^\flat$:

$$\frac{dc_i}{dt} = \iint_M \omega [\![\mathbf{h}_i, \mathbf{u}]\!] \, dA - \nu \langle\!\langle \mathbf{h}_i^\flat, \delta\omega \rangle\!\rangle + 2\nu \iint_M \langle \mathbf{h}_i, \mathbf{u} \rangle K \, dA. \tag{34}$$

The middle term $\langle\!\langle \mathbf{h}_i^\flat, \delta\omega \rangle\!\rangle$ can be expanded as

$$-\langle\!\langle \mathbf{h}_i^\flat, \delta\omega \rangle\!\rangle = -\iint_M \mathbf{h}_i^\flat \wedge dw = \iint_M d(w\mathbf{h}_i^\flat) = \oint_{\partial M} w\mathbf{h}_i^\flat \tag{35}$$

using $\delta\omega = \star^{-1} d \star \omega$, $\langle\!\langle \cdot, \cdot \rangle\!\rangle = \iint_M (\cdot) \wedge \star(\cdot)$, $d\mathbf{h}_i^\flat = 0$, $\star\omega = w$, and Stokes' theorem. Thus, we obtain:

$$\boxed{\frac{dc_i}{dt} = \iint_M \Big((\mathbf{h}_i \times \mathbf{u}) w + 2\nu \langle \mathbf{h}_i, \mathbf{u} \rangle K \Big) \, dA + \oint_{\partial M} \nu h_{i\partial} w \, ds} \tag{36}$$

where $h_{i\partial}$ is the tangential component of $\mathbf{h}_i$ along the boundary:

$$h_{i\partial} \colon \partial M \to \mathbb{R}, \quad h_{i\partial} \coloneqq \langle \mathbf{h}_i, \mathbf{t} \rangle \tag{37}$$

with $\mathbf{t}$ being the unit tangent vector for the oriented curve ∂M. In two dimensions, the cross product $\times$ of two tangent vectors is a scalar, defined by $\mathbf{h}_i \times \mathbf{u} \coloneqq \langle J\mathbf{h}_i, \mathbf{u} \rangle$.

Remark 2.5 (Interior and boundary viscous effects on the harmonic part)**.** *If $\partial M = \varnothing$, the boundary term $\oint_{\partial M} \nu h_{i\partial} w \, ds$ vanishes. In this case, the only remaining viscous contribution to $\frac{dc_i}{dt}$ is the curvature term $\iint_M 2\nu \langle \mathbf{h}_i, \mathbf{u} \rangle K \, dA$. In general, the only interior viscous contribution to $\frac{dc_i}{dt}$ is the curvature term, while the diffusion term contributes solely through the boundary.*

2.3.4 Summary. The vorticity formulation for the Navier–Stokes equation can be summarized as follows. The state variables are the vorticity scalar field $w \in \Omega^0(M)$ and the coefficients $c_1, \ldots, c_m \in \mathbb{R}$, all depending on time. Each state $(w, c_1, \ldots, c_m)$ determines a unique velocity vector field $\mathbf{u}$ via (31), which requires solving the scalar Poisson problem (32) together with a fixed orthonormal basis $(\mathbf{h}_1, \ldots, \mathbf{h}_m)$ for harmonic fields.

Theorem 2.4. *Under the Navier–Stokes equation* (11)*, the variables $(w, c_1, \ldots, c_m)$ evolve according to*

$$\boxed{\begin{cases} \frac{\partial w}{\partial t} + \mathbf{u} \cdot \nabla w = \nu \Delta w + 2\nu \operatorname{curl}(K\mathbf{u}), \\ \frac{dc_i}{dt} = \iint_M [(\mathbf{h}_i \times \mathbf{u}) w + 2\nu (\mathbf{h}_i \cdot \mathbf{u}) K] \, dA + \oint_{\partial M} \nu h_{i\partial} w_\partial \, ds. \end{cases}} \tag{38}$$

We emphasize that the evolution system (38) remains incomplete until additional boundary conditions are specified.

Remark 2.6. *The evolution system* (38) *is not yet complete because certain variables on the right-hand side remain undetermined. Specifically, the boundary value $w|_{\partial M}$ of the vorticity is required. Note that the vorticity equation in* (38) *governs only the interior of M and provides no direct information about $w|_{\partial M}$. These boundary values are necessary both for evaluating the diffusion term $\nu\Delta w$ in the vorticity equation and for computing the boundary integral $\oint_{\partial M} \nu h_{i\partial} w_\partial \, ds$. The remaining components of the system, including* (31) *and* (32)*, involve only the interior values of w.*

3 BOUNDARY CONDITIONS

As discussed in Remark 2.6, the boundary vorticity $w_\partial \colon \partial M \to \mathbb{R}$ is an unknown function appearing on the right-hand side of the evolution equation (38). An additional set of equations is required to constrain the freedom of w_∂ at each time t. In this section, we detail how three common boundary conditions—free-slip, friction, and no-slip—are incorporated into (38). In particular, we show that the curvature of the boundary plays a crucial role in these conditions.

3.1 Free-Slip Boundary

The free-slip boundary condition is the mathematical *natural boundary condition* derived from the Rayleigh variational principle in Section 2.1.2. It is also known as the *Navier slip condition.*

Definition 3.1 (Natural boundary condition)**.** *Let $(\operatorname{grad}\mathcal{F})|_{\mathbf{u}} \in \mathfrak{X}_{\mathrm{div}}$ be the gradient of a functional $\mathcal{F} \colon \mathfrak{X}_{\mathrm{div}} \to \mathbb{R}$ at $\mathbf{u} \in \mathfrak{X}_{\mathrm{div}}$ as defined in Definition 2.3. The* ***natural boundary condition*** *associated with $\mathcal{F}$ is the condition on $\mathbf{u} \in \mathfrak{X}_{\mathrm{div}}$ such that* (9) *continues to hold for any variation $\mathring{\mathbf{u}} \in \mathfrak{X}_{\mathrm{div}}$ without requiring $\mathring{\mathbf{u}}$ to vanish on ∂M.*

Proposition 3.1. *The natural boundary condition for $\mathcal{R}$, defined in* (8)*, is:*

$$\boxed{(\mathcal{K}\mathbf{u})[\![\mathbf{t}, \mathbf{n}]\!] = 0} \quad \text{on } \partial M, \tag{39}$$

where $\mathbf{t}$ is the unit tangent of the oriented curve ∂M, and $\mathbf{n} = J\mathbf{t}$.

Proof. Appendix A.5. □

Physically, the condition $(\mathcal{K}\mathbf{u})[\![\mathbf{t}, \mathbf{n}]\!] = 0$ expresses the absence of friction. The application $(\mathcal{K}\mathbf{u})[\![\mathbf{n}, \cdot]\!]$ of the tensor $\mathcal{K}\mathbf{u}$ on $\mathbf{n}$ represents the traction force (up to a factor of 2ν) exerted on the boundary geometry ∂M (whose normal is $\mathbf{n}$). Thus, the condition $(\mathcal{K}\mathbf{u})[\![\mathbf{t}, \mathbf{n}]\!] = 0$ states that this traction force has no tangential component, meaning there is no friction or shear stress from the boundary, allowing the fluid to slip freely along the wall.

Theorem 3.1. *Under the natural boundary condition* (39)*, the boundary vorticity is:*

$$\boxed{w_\partial = 2\kappa_{\mathrm{g}} u_\partial} \quad \text{on } \partial M \tag{40}$$

where $u_\partial \coloneqq \langle \mathbf{u}, \mathbf{t} \rangle \colon \partial M \to \mathbb{R}$ is the tangential velocity component, and κ_{g} is the geodesic curvature of ∂M.

Proof. Appendix C.1 □

Example 3.1. *The rigid rotating flow in a circular disk serves as an analytical example of* (40)*. On the disk of radius R centered at the origin, a rigid rotation with angular velocity a induces a velocity field $(u_x, u_y) = a(-y, x)$, corresponding to a constant vorticity $w = 2a$. The*

boundary velocity is $u_\partial = Ra$ and the boundary curvature is $\kappa_g = \frac{1}{R}$. One can verify $w = 2\kappa_g u_\partial$.

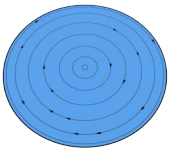

Equation (40) can be directly substituted into (38). The boundary integral $\oint_{\partial M} \nu h_i \partial w_\partial \, ds$ becomes $\oint_{\partial M} 2\nu h_i \partial u_\partial \kappa_g \, ds$. We can reorganize the resulting equation geometrically using the following notion.

Definition 3.2 (Gauss–Bonnet curvature density)**.** *The **Gauss–Bonnet curvature density** is a distributional 2-form $\Omega \in \Omega^2(M)$ defined by:*

$$\iint_M f\Omega \coloneqq \iint_M fK \, dA + \oint_{\partial M} f\kappa_g \, ds \tag{41}$$

for any smooth function $f \in C^\infty(M)$.

Formally, Ω can be written as $\Omega = (K + \kappa_g \delta_{\partial M}) \, dA$ where $\delta_{\partial M}$ is the Dirac δ-distribution supported on ∂M. Ω serves as the integrand in the Gauss–Bonnet theorem, satisfying $\iint_M \Omega = 2\pi\chi(M)$, where $\chi(M)$ is the Euler characteristic of M. Thus, Ω generalizes the Gaussian curvature 2-form to surfaces with boundaries, ensuring that integration yields a topological invariant as in the classical Gauss–Bonnet theorem for closed surfaces.

Corollary 3.1. *Under the Navier–Stokes equation* (11) *and the free-slip boundary condition* (39)*, the harmonic coefficients $(c_1, \dots, c_m)$ evolve according to:*

$$\boxed{\frac{dc_i}{dt} = \iint_M (\mathbf{h}_i \times \mathbf{u})\omega + 2\nu(\mathbf{h}_i \cdot \mathbf{u})\Omega.} \tag{42}$$

Remark 3.1. *While the relationship* (40) *is consistent with the general understanding that boundary curvature and tangential velocity contribute to vorticity generation, a specific formulation equating boundary vorticity to the product of geodesic curvature and tangential velocity is not commonly found in standard references. One appearance of* (40) *can be found in [Kelliher 2006]. We speculate that the result of Corollary 3.1 may lead to a mathematically rigorous foundation for the **Kutta condition**, which argues that steady flows around an airfoil are typically accompanied by a circulation such that the tangential velocity vanishes near the airfoil's tail, where $\kappa_g = \infty$. See Figure 5.*

In fact, the boundary condition (40) can be elegantly absorbed into the vorticity equation using the Gauss–Bonnet curvature density Ω. Note that the Gauss–Bonnet curvature K^Ω, defined by

$$\Omega = (K + \kappa_g \delta_{\partial M}) \, dA =: K^\Omega \, dA, \tag{43}$$

exhibits a singular curvature sheet along the boundary, as discussed in Remark 2.3. Theorem 2.3 shows that if we replace K by K^Ω in (28), a jump $[w]_{\partial M} = 2\kappa_g u_\partial$ arises naturally. To exploit this, we set the Dirichlet boundary condition $w|_{\partial M} = 0$. The vorticity just inside the boundary then matches $2\kappa_g u_\partial$, consistent with (40).[4]

Corollary 3.2. *The vorticity equation* (28) *with the free-slip condition* (40) *is equivalent to the vorticity equation with using Gauss–Bonnet curvature $K^\Omega = K + \kappa_g \delta_{\partial M}$ with the zero Dirichlet boundary condition:*

$$\begin{cases} \frac{\partial w}{\partial t} + \mathbf{u} \cdot \nabla w = \nu \Delta w + 2\nu \operatorname{curl}(K^\Omega \mathbf{u}), \\ w|_{\partial M} = 0 \end{cases} \tag{44}$$

That is, an equivalent formulation of the Navier–Stokes equation (11) *with the free-slip boundary condition* (39) *is the evolution of $(w, c_1, \dots, c_m)$ governed by*

$$\boxed{\begin{cases} \frac{\partial w}{\partial t} + \mathbf{u} \cdot \nabla w = \nu \Delta w + 2\nu \operatorname{curl}(K^\Omega \mathbf{u}), \\ \frac{dc_i}{dt} = \iint_M (\mathbf{h}_i \times \mathbf{u})\omega + 2\nu(\mathbf{h}_i \cdot \mathbf{u})\Omega, \\ w|_{\partial M} = 0. \end{cases}} \tag{45}$$

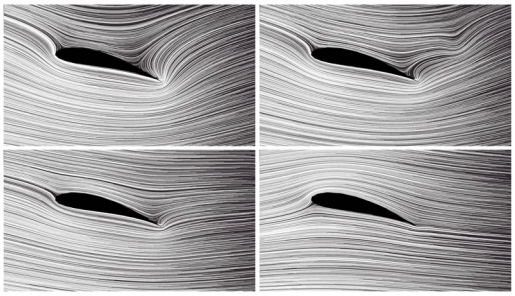

Fig. 5. The effect of boundary curvature on viscous flow around an obstacle with free-slip boundary condition. The flow around an airfoil with free-slip boundary exhibits nontrivial evolution in its harmonic component. In particular, circulation around the airfoil increases to satisfy the *Kutta condition*—ensuring that the flow does not wrap about the sharp trailing edge. The simulation is performed using Algorithm 1, which solves (45), on a cylindrical surface with an embedded airfoil-shaped region removed.

3.2 Navier Friction Boundary

The natural boundary condition (39) imposes zero shear stress at the boundary. If instead there is friction from the wall, the boundary condition becomes:

$$\boxed{2\nu(\mathcal{K}\mathbf{u})[\![\mathbf{t}, \mathbf{n}]\!] = \alpha u_\partial} \quad \text{on } \partial M \tag{46}$$

where $\alpha > 0$ is the friction coefficient.

Theorem 3.2. *Under the friction condition* (46)*, the boundary vorticity is:*

$$\boxed{w_\partial = (2\kappa_g - \tfrac{\alpha}{2\nu})u_\partial} \quad \text{on } \partial M, \tag{47}$$

where u_∂ is the tangential velocity component, and κ_g is the geodesic curvature of ∂M.

Proof. Appendix C.2 □

Equation (47) is consistent with the general understanding that for large relative friction ($\alpha/\nu \gg 0$), vorticity generation is approximately proportional to the negative of the tangential velocity [Lighthill 1963; Chorin 1978]. Equation (47) precisely specifies that this proportionality constant is the relative friction coefficient offset by the geodesic curvature of the boundary [Kelliher 2006].

Similar to the treatment of the free-slip condition using the Gauss–Bonnet curvature (Definition 3.2), we can incorporate the condition

[4]Here, the jump $[w]_{\partial M}$ of vorticity is evaluated with the vorticity on the outer side of ∂M set to zero, as prescribed by the Dirichlet condition. This is because the singular curvature sheet $\kappa_g \delta_{\partial M}$ is supported slightly inside the domain, which is consistent with the discrete setting described in (62) in Section 5.1.3, where the curvature sheet is supported along the triangle strip adjacent to the boundary.

Fig. 6. On the Schwarz P surface, an initially stationary fluid ($w = 0$, $\mathbf{c} = \mathbf{0}$) is set into motion by a rotating boundary with prescribed velocity $\bar{u}_\partial = 2$. The no-slip condition (52) is enforced using Alg. 2 with time step $\Delta t = 0.01$. Each boundary circle has radius 0.4, and the viscosity is set to $\nu = 0.01$.

(47) using a modified Gauss–Bonnet curvature. Specifically, we shift the geodesic curvature by the factor $\frac{\alpha}{4\nu}$.

Definition 3.3 (Gauss–Bonnet curvature with friction). *The **Gauss–Bonnet curvature density with friction** $\frac{\alpha}{4\nu}$ is a distributional 2-form $\Omega^{\alpha/(4\nu)}$ defined by*

$$\iint_M f\,\Omega^{\alpha/(4\nu)} \coloneqq \iint_M f K\,dA + \oint_{\partial M} f(\kappa_g - \tfrac{\alpha}{4\nu})\,ds \tag{48}$$

for any smooth function $f \in C^\infty(M)$. The associated curvature function $K^{\Omega,\alpha/\nu}$ is defined by

$$K^{\Omega,\alpha/(4\nu)} \coloneqq K + (\kappa_g - \tfrac{\alpha}{4\nu})\delta_{\partial M}, \quad \Omega^{\alpha/(4\nu)} = K^{\Omega,\alpha/(4\nu)}\,dA. \tag{49}$$

Corollary 3.3. *An equivalent formulation of the Navier–Stokes equation* (11) *with the Navier friction boundary condition* (46) *is the evolution of $(w, c_1, \ldots, c_m)$ governed by*

$$\boxed{\begin{cases} \frac{\partial w}{\partial t} + \mathbf{u}\cdot\nabla w = \nu\Delta w + 2\nu\,\mathrm{curl}(K^{\Omega,\alpha/(4\nu)}\mathbf{u}), \\ \frac{dc_i}{dt} = \iint_M (\mathbf{h}_i \times \mathbf{u})\omega + 2\nu(\mathbf{h}_i\cdot\mathbf{u})\Omega^{\alpha/(4\nu)}, \\ w|_{\partial M} = 0. \end{cases}} \tag{50}$$

3.3 No-Slip Boundary

The no-slip boundary condition is defined by

$$\boxed{u_\partial = 0} \quad \text{on } \partial M, \tag{51}$$

where u_∂ denotes the tangential velocity at ∂M. The condition can be generalized to

$$u_\partial = \bar{u}_\partial \quad \text{on } \partial M, \tag{52}$$

where $\bar{u}_\partial$ is a prescribed tangential velocity that can be nonzero. Condition (51) can be viewed as the limiting case of the Navier friction condition (46) as $\alpha/\nu \to \infty$. Unlike the free-slip condition (40) or the friction condition (47), the no-slip condition (51) does not directly prescribe the the boundary vorticity w_∂. Instead, the boundary vorticity is determined implicitly through the system's dynamics. In the computational setting, the boundary vorticity is characterized as follows:

> *The boundary vorticity $w_\partial\colon \partial M \to \mathbb{R}$ is chosen so that, after one time step of simulating the full system* (38) *using this boundary vorticity, the reconstructed velocity* (31) *satisfies $u_\partial = 0$.*

This implicit step is implemented by a fixed point iteration as detailed in Section 5.3.2. Figure 6 shows an example of (52) imposed on a surface with moving boundary.

3.3.1 Discussion. Incorporating the no-slip boundary condition into the vorticity formulation is not straightforward. There is a long history of research on this topic [Gresho 1991; Rempfer 2006]. Here, we briefly review key developments and clarify certain points, particularly revising some statements where harmonic components were typically neglected in prior work.

The no-through and no-slip conditions translate into $\psi = \frac{\partial\psi}{\partial\mathbf{n}} = 0$ for the streamfunction ψ at the boundary.[5] Early approaches imposed $\Delta\psi = w$ together with $\psi = \frac{\partial\psi}{\partial\mathbf{n}} = 0$ at the boundary. Thom [1933], Roache [1976], and others (see the comprehensive review by E and Liu [1996]) set $w_\partial = \Delta\psi|_{\partial M}$. However, these conditions were later shown to be overdetermined. To address this, E and Liu [1996] suggested imposing $w_\partial = \Delta\psi|_{\partial M}$ in an explicit time-splitting scheme, noting that it produces roughly the correct amount of vortex sheet.

The problem of overdetermined boundary condition $\psi = \frac{\partial\psi}{\partial\mathbf{n}} = 0$ was pointed out by [Quartapelle 1981; Quartapelle and Valz-Gris 1981]. This overdetermination constraints the vorticity field w to a smaller admissible subspace. Explicitly, it requires that w *be L^2-orthogonal to all harmonic functions on M*. However, this characterization did not consider harmonic components and thus fails in non-simply-connected domains. Here, we provide a revised version of the Quartapelle–Valz-Gris condition:

Theorem 3.3 (Revised Quartapelle–Valz-Gris condition). *For each $f\colon \partial M \to \mathbb{R}$, let $\phi_f\colon M \to \mathbb{R}$ denote its harmonic extension to the interior, defined by the Dirichlet problem $\Delta\phi_f = 0$ with $\phi_f|_{\partial M} = f$. Under the Navier–Stokes equations with the no-slip condition, the vorticity w and the harmonic coefficients $(c_1, \ldots, c_m)$ satisfy*

$$\iint_M \phi_f w\,dA + \sum_{i=1}^m c_i \oint_{\partial M} f h_{i\partial}\,ds = 0 \tag{53}$$

for all $f\colon \partial M \to \mathbb{R}$.

Proof. See Appendix C.3. □

A modern understanding of the vorticity and the no-slip condition emphasizes that vortices are generated at the boundary to maintain the no-slip condition. Lighthill [1963] proposed vorticity generation proportional to the negative of the slip velocity. Chorin [1973; 1978; 1980] developed vortex sheet boundary layer models aligned with Lighthill's ideas. Anderson [1989] showed that the vorticity flux from the boundary can be derived from the Quartapelle–Valz-Gris condition. See also [Koumoutsakos et al. 1994; Kempka et al. 1995]. Our implicit solve for the no-slip condition follows this general approach.

Cottet [1988; 2000] introduces a different method, recently adopted by [Wang et al. 2024] in the computer graphics community. Rather than using a streamfunction, Cottet reconstructs velocity from vorticity via the equation $(d\delta + \delta d)\mathbf{u}^\flat = \delta\omega$ with $\mathbf{u} = \mathbf{0}$ on the boundary. This equation does not directly imply the divergence-free condition $\delta\mathbf{u}^\flat = 0$. Cottet additionally suggests imposing $\omega = d\mathbf{u}^\flat$ at the boundary in the convection-diffusion equation for vorticity.

[5] The condition $\psi = \frac{\partial\psi}{\partial\mathbf{n}} = 0$ is no longer strictly true in the presence of harmonic components. With harmonic components included, the condition becomes $\psi = \frac{\partial\psi}{\partial\mathbf{n}} + \sum_{i=1}^m c_i h_{i\partial} = 0$.

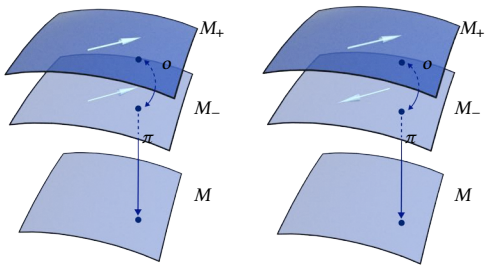

Fig. 7. Even (left) and odd (right) vector fields on $\widetilde{M}$

This is implemented as a Neumann condition $\frac{\partial w}{\partial \mathbf{n}} = \frac{\partial}{\partial \mathbf{n}}(\operatorname{curl} \mathbf{u}) - \frac{1}{|\partial M|}\oint_{\partial M} \frac{\partial}{\partial \mathbf{n}}(\operatorname{curl} \mathbf{u})$, where the mean-removal term is to enforce $\iint \omega = 0$ at all time, based on the circulation theorem (or as a special case of the classical Quartapelle–Valz-Gris condition).

Wang et al. [2024] recently applied Cottet's boundary treatment in graphics. They use it for the velocity reconstruction via $-\Delta \mathbf{u} = \operatorname{grad} w$ (in 2D) with $\mathbf{u} = \mathbf{0}$ at the boundary. In this Poisson problem adjacent to the boundary, the value of w_∂ is required; they set $w_\partial = \operatorname{curl} \mathbf{u}$ by back-referencing the velocity, forming a modified Poisson equation [Wang et al. 2024, § 4.1–4.2]. However, this system is degenerate when the domain is non-simply-connected [Wang et al. 2024, § 7]. Although their solver appears to select solutions that yield qualitatively reasonable dynamics [Wang et al. 2024, Fig. 11], the scheme enforces only $\mathbf{u} \cdot \mathbf{n} = 0$ and the tangential part of the velocity is not fully constrained.

4 NON-ORIENTABLE SURFACES

The core theory presented in the preceding sections assumes that the surface M is orientable. The 90° rotation operator $\mathcal{J}$ and the Hodge stars $\star$ both depend on the orientation of M. In particular, the vorticity function, defined as the Hodge star of the vorticity 2-form, is not globally well-defined on non-orientable surfaces, as its sign flips when traversing, *e.g.*, a Möbius strip. Nevertheless, fluids can flow on both orientable and non-orientable surfaces. How, then, can we apply the vorticity formulation on a non-orientable surface?

In this section, we extend our theory to fluids on non-orientable surfaces by introducing a useful technique: doubling the domain M to obtain a closed, orientable surface $\widetilde{M}$. We show that solving the Navier–Stokes equations on $\widetilde{M}$ is equivalent to solving them on M. This approach enables fluid simulations on a non-orientable surface M by solving Navier–Stokes equation on its orientable double cover $\widetilde{M}$. The formulation also provides a new perspective on the natural boundary condition (40) (Section 4.3).

4.1 Double Cover

The following construction of ***double cover*** turns any surface M with boundary and any closed non-orientable surface M into a *closed orientable* surface $\widetilde{M}$.

Case 1 *M is orientable and has boundary.* The double cover $\widetilde{M}$ is constructed by taking two copies of M and gluing their corresponding boundary points together. More precisely, let $M_+, M_- \simeq M^\circ$ be two copies of the interior of M, and let $\Gamma \simeq \partial M$ be a copy of the boundary. Define $\widetilde{M} \coloneqq M_+ \sqcup \Gamma \sqcup M_-$, and let $\pi\colon \widetilde{M} \to M$ be the projection that maps each $x \in \widetilde{M}$ to the point in M from which it was copied. The topology of $\widetilde{M}$ is defined so that π is continuous.

Case 2 *M is non-orientable.* Let $\widetilde{M}$ be the standard oriented double cover of M with the boundary points glued together. A concrete construction goes as follows. Choose a set of curves $C \subset M^\circ$ as cuts in the interior M° of M, so that $M' \coloneqq M^\circ \setminus C$ is orientable (*i.e.*, M' is a maximal oriented subdomain of M°).[6] Let $M'_+, M'_- \simeq M'$ be two copies of M', let $C_+, C_- \simeq C$ be two copies of C, and let $\Gamma \simeq \partial M$ be a copy of the boundary (which may be empty). Define $\widetilde{M} \coloneqq M'_+ \sqcup M'_- \sqcup C_+ \sqcup C_- \sqcup \Gamma$, and let $\pi\colon \widetilde{M} \to M$ be the projection that sends each $x \in \widetilde{M}$ to the point in M from which it originates.

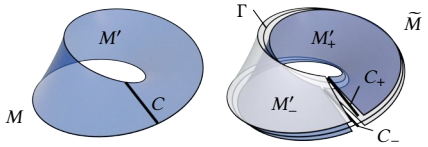

The topology of $\widetilde{M}$ is defined so that it is orientable—meaning, in particular, that C_+ is adjacent to M'_+ on one side and M'_- on the other—and such that π is continuous. The resulting object $(\widetilde{M}, \pi)$ is independent of the choice of the cuts C.

Note that $\widetilde{M}$ is always an orientable closed surface by construction. If M is orientable with genus g and b boundary components, then $\operatorname{genus}(\widetilde{M}) = 2g + \max(b-1, 0)$. If M is non-orientable and is the connected sum of k real projective planes with b disks removed, then $\operatorname{genus}(\widetilde{M}) = k - 1 + b$.

The double cover $(\widetilde{M}, \pi)$ is naturally equipped with an involutive map $o\colon \widetilde{M} \to \widetilde{M}$ that swaps the corresponding points in M_+ and M_- for orientable M, and swaps the corresponding points in M'_+, M'_- and C_+, C_- for non-orientable M. Explicitly, o is defined by $\pi \circ o = \pi$, and $o(x) \neq x$ for $x \notin \Gamma$. The map o is an involution, *i.e.*, $o^2 = \mathrm{id}_{\widetilde{M}}$, and Γ is the set of fixed points of o.

Both π and o are isometries.

4.1.1 Curvature of $\widetilde{M}$. Since M_+ and M_- (resp. M'_+ and M'_-) are isometric to M° (resp. M'), the Gaussian curvature on $\widetilde{M} \setminus \Gamma$ is given by $K \circ \pi$. We may abbreviate $K \circ \pi$ as K since they have the same values. However, the Gaussian curvature $\widetilde{K}$ of $\widetilde{M}$ is not simply K everywhere. The interface Γ forms a sharp ridge, with concentrated Dirac-δ Gaussian curvature. Precisely:

$$\widetilde{K} = K + 2\kappa_{\mathrm{g}}\delta_\Gamma. \tag{54}$$

4.1.2 Even and Odd Fields. The map $o\colon \widetilde{M} \to \widetilde{M}$ induces a pullback operator o^* that acts on fields. These fields can be scalar functions $\Omega^0(\widetilde{M})$, vector fields $\mathfrak{X}(\widetilde{M})$, or differential forms $\Omega^k(\widetilde{M})$. The pullback o^* is linear and involutive (since o is an involution). Thus, the eigenvalues of o^* are ± 1. We refer to elements of the $+1$-eigenspace as ***even field***, and to elements of the -1-eigenspace as ***odd field***.

[6] In practice, for a mesh M, one may use a spanning tree to orient the faces of M, with C given by the edges where adjacent faces remain inconsistently oriented.

Fig. 8. Among the two-dimensional space of harmonic fields on the torus—the oriented double cover of the Klein bottle—only one dimension, corresponding to the even harmonic field, contributes to the harmonic vector field on the Klein bottle, as shown on the left. The other dimension, spanned by an odd harmonic field, does not descend to the Klein bottle, as illustrated on the right by the visible discontinuity.

That is, an even field f satisfies $o^*f = f$, and an odd field satisfies $o^*f = -f$.[7]

Every field f admits a unique decomposition into even and odd parts: $f = \frac{f+o^*f}{2} + \frac{f-o^*f}{2}$.

Even functions take the same value at opposite points, while odd functions take values of equal magnitude but opposite sign. In particular, odd functions vanish on Γ.

Even vector fields $\mathbf{v}$ satisfy $do(\mathbf{v}) = \mathbf{v}$; odd ones satisfy $do(\mathbf{v}) = -\mathbf{v}$. See Figure 7. Divergence-free even vector fields must be tangent to Γ. In particular, $\mathfrak{X}_{\mathrm{div}}(M) \cong \mathfrak{X}_{\mathrm{div,even}}(\widetilde{M})$.

The operators $\sharp, \flat, d$, grad, div preserve the evenness and oddness. The Hodge star $\star$ and the 90° rotation operator J switch the even/odd parity. Wedge product and inner product respect the parity: even · even = odd · odd = even, and even · odd = odd.

4.1.3 Hodge Decomposition. Since the exterior calculus operators respect parity, the Hodge decomposition respects the even/odd splitting. Note that 1-forms on M satisfying the co-Dirichlet (Neumann) boundary condition correspond to $\Omega^1_{\mathrm{even}}(\widetilde{M})$, and 1-forms satisfying the Dirichlet boundary condition correspond to $\Omega^1_{\mathrm{odd}}(\widetilde{M})$. These admit the Hodge decomposition:

$$\Omega^1_{\mathrm{even}}(\widetilde{M}) = d\Omega^0_{\mathrm{even}}(\widetilde{M}) \oplus \delta\Omega^2_{\mathrm{even}}(\widetilde{M}) \oplus \mathcal{H}^1_{\mathrm{even}}(\widetilde{M}), \tag{55}$$

$$\Omega^1_{\mathrm{odd}}(\widetilde{M}) = d\Omega^0_{\mathrm{odd}}(\widetilde{M}) \oplus \delta\Omega^2_{\mathrm{odd}}(\widetilde{M}) \oplus \mathcal{H}^1_{\mathrm{odd}}(\widetilde{M}). \tag{56}$$

The space of velocity 1-forms $\mathfrak{X}_{\mathrm{div}}(M)^\flat$ corresponds to $\delta\Omega^2_{\mathrm{even}}(\widetilde{M}) \oplus \mathcal{H}^1_{\mathrm{even}}(\widetilde{M})$. Thus, harmonic vector fields in $\mathfrak{X}_{\mathrm{div}}(M)$ correspond to even harmonic 1-forms, while streamfunctions are odd functions (or equivalently, even 2-forms).

If M is non-orientable, its double cover $\widetilde{M}$ has $2 \cdot \mathrm{genus}(\widetilde{M})$ linearly independent harmonic 1-forms, half of which are even. For example, the Klein bottle is double-covered by a torus. The torus has a 2D space of harmonic fields—one even and one odd—so only one harmonic field contributes to the harmonic velocity on the Klein bottle. See Figure 8.

[7] Odd differential forms are sometimes referred to as *pseudoforms*, *twisted forms*, or forms of *odd type*, as introduced in de Rham's work [1984].

Field	Symbol	Type
Velocity	$\mathbf{u}$	even div-free vector field
Velocity 1-form	$\mathbf{u}^\flat$	even 1-form
Vorticity function	w	odd function
Vorticity 2-form	ω	even 2-form
Streamfunction	ψ	odd function
Harmonic fields	$\mathbf{h}_i$	even harmonic vector field
Gaussian curvature	$\widetilde{K}$	even function
Gaussian curvature density	$\widetilde{\Omega}$	even density or odd 2-form

Table 1. Type of fields on the double cover $\widetilde{M}$.

4.2 Navier–Stokes Equations on the Double Cover

Each quantity in the Navier–Stokes system on M lifts to either an even or odd field on $\widetilde{M}$, as summarized in Table 1. If the initial data respect this parity structure, then the evolution under the Navier–Stokes equations preserves it.

This means our Navier–Stokes formulation for orientable surfaces directly extends to non-orientable ones, by simulating the dynamics on the orientable double cover using initial data with the parity structure described in Table 1.

4.3 Relation to Boundary Conditions

As shown in (54), the Gaussian curvature of $\widetilde{M}$ contains a singular curvature sheet along Γ. By Theorem 2.3, the vorticity function w exhibits a jump across Γ:

$$[w]_\Gamma = 4\kappa_g u_\partial. \tag{57}$$

Since w is an odd function on $\widetilde{M}$, it vanishes at Γ , and has opposite limiting values from either side: $2\kappa_g u_\partial$ from M^+, and $-2\kappa_g u_\partial$ from M^-. Thus, we recover the natural (free-slip) boundary condition (40) on M automatically.

To simulate Navier friction or no-slip boundary conditions on M using $\widetilde{M}$, one cuts Γ open, thereby turning $\widetilde{M}$ into a surface with boundary, and imposes the desired boundary condition on $\partial\widetilde{M}$.

5 DISCRETIZATION

Our numerical method for simulating (38) is based on the discretization following [Azencot et al. 2014] and [Yin et al. 2023].

For spatial discretization, the surface M is represented by a triangle mesh (P, E, F), where P is the set of vertices, E the set of edges, and F the set of faces. The vorticity function w and the streamfunction ψ are discretized at vertices, while the vector fields $\mathbf{u}, \mathbf{h}_i$ are discretized on faces. The discrete Gauss–Bonnet curvature is also assigned to faces. Details of the discrete operators and the face-based discrete Gauss–Bonnet curvature are provided in Section 5.1.

For time integration, we employ an *implicit-explicit (IMEX) scheme*. Specifically, we split the system into a *stiff part* and a *non-stiff part*. The stiff part consists of the viscous term $\nu(\Delta w + 2\,\mathrm{curl}(K\mathbf{u}))$ in the vorticity equation, while the remaining terms in the vorticity equation and the evolution equation of the harmonic components are classified as non-stiff. The non-stiff part is integrated with an explicit 4th-order Runge–Kutte (RK4) method [Yin et al. 2023], alternating

with an implicit backward Euler method applied to the stiff viscous term. The full procedure is described in Section 5.2.

For simplicity, we first present the method for system with the free-slip boundary condition; the incorporation of the friction and no-slip boundary conditions is described separately in Section 5.3.

5.1 Discrete Surface and Its Operators

5.1.1 Discrete Differential Operators. A discrete vector field $\mathbf{u} \in \Gamma_{\mathsf{F}}(TM)$ is defined as a piecewise constant vector $\mathbf{u}_{\mathsf{f}} \in T_{\mathsf{f}}M$ assigned on each triangle $\mathsf{f} \in \mathsf{F}$. The directional derivative operator associated with $\mathbf{u}$, denoted as $[\nabla_{\mathbf{u}}] : \mathbb{R}^{|\mathsf{P}|} \to \mathbb{R}^{|\mathsf{P}|}$, acts on a discrete function $f = (f_{\mathsf{p}})_{\mathsf{p}\in\mathsf{P}} \in \mathbb{R}^{|\mathsf{P}|}$ as

$$([\nabla_{\mathbf{u}}]f)_{\mathsf{p}} \coloneqq \frac{1}{\sum_{\mathsf{f}\succ\mathsf{p}} A_{\mathsf{f}}} \sum_{\mathsf{f}\succ\mathsf{p}} A_{\mathsf{f}} \langle \mathbf{u}_{\mathsf{f}}, (\operatorname{grad} f)_{\mathsf{f}} \rangle \tag{58}$$

where A_{f} is the area of triangle f, and $\operatorname{grad} : \mathbb{R}^{|\mathsf{P}|} \to \Gamma_{\mathsf{F}}(TM)$ computes the piecewise constant gradient of the linear interpolation of the discrete function f.

The divergence operator $\operatorname{div} : \Gamma_{\mathsf{F}}(TM) \to \mathbb{R}^{|\mathsf{P}|}$ is defined as the negative L^2-adjoint of the gradient, $\operatorname{div} = -\operatorname{grad}^*$. Explicitly, $\operatorname{div} = -A_{\mathsf{P}}^{-1} \operatorname{grad}^{\mathsf{T}} A_{\mathsf{F}}$ where A_{F} is the diagonal matrix of triangle areas, and A_{P} is the diagonal matrix of the vertex areas.

The scalar curl operator is defined as the composition of the divergence with the facewise 90° counterclockwise rotation: $J_{\mathsf{F}}\mathbf{u} = (J_{\mathsf{f}}\mathbf{u}_{\mathsf{f}})_{\mathsf{f}\in\mathsf{F}}$. That is, $\operatorname{curl} = -\operatorname{div} \circ J_{\mathsf{F}} : \Gamma_{\mathsf{F}}(TM) \to \mathbb{R}^{|\mathsf{P}|}$.

The Laplacian $\Delta = \operatorname{div} \circ \operatorname{grad} : \mathbb{R}^{|\mathsf{P}|} \to \mathbb{R}^{|\mathsf{P}|}$ corresponds to the cotangent Laplacian on mesh M. When assembled in matrix form, it takes the form $\Delta = -A_{\mathsf{P}}^{-1} L \in \mathbb{R}^{|\mathsf{P}|\times|\mathsf{P}|}$, where $L = \operatorname{grad}^{\mathsf{T}} A_{\mathsf{F}} \operatorname{grad}$ is the cotangent stiffness matrix.

5.1.2 Interior and Boundary Vertices. We decompose the vertex set into the interior and boundary parts: $\mathsf{P} = \mathsf{I} \sqcup \mathsf{B}$, where I and B denote the interior and boundary vertex sets. If M is a closed surface, then $\mathsf{P} = \mathsf{I}$ and $\mathsf{B} = \varnothing$.

5.1.3 Discrete Gauss Curvature. We discretize Gaussian curvature at faces as the total *angle defect* divided by the triangle area, defined as follows.

For each vertex p incident to face f, let $\angle_{\mathsf{p},\mathsf{f}}$ denote the interior angle of the triangle f at vertex p. Define the *rescaled interior angle* as

$$\tilde{\angle}_{\mathsf{p},\mathsf{f}} \coloneqq \begin{cases} \frac{2\pi}{\sum_{\mathsf{f}'\succ\mathsf{p}} \angle_{\mathsf{p},\mathsf{f}'}} \angle_{\mathsf{p},\mathsf{f}} & \text{for } \mathsf{p} \in \mathsf{I} \\ \angle_{\mathsf{p},\mathsf{f}} & \text{for } \mathsf{p} \in \mathsf{B}. \end{cases} \tag{59}$$

This angle is rescaled in the sense that the total angle around an interior vertex is $\sum_{\mathsf{f}\succ\mathsf{p}} \tilde{\angle}_{\mathsf{p},\mathsf{f}} = 2\pi$. Geometrically, $\tilde{\angle}_{\mathsf{p},\mathsf{f}}$ is the geodesic corner angle obtained by smoothing the vertex cone and measuring angles in the tangent plane at the vertex. This modification of angle, however, no longer satisfies the total interior angle of a triangle being π, and thereby renders a total angle defect in each triangle. For each triangle $\mathsf{f} \in \mathsf{F}$, define the *discrete Gaussian curvature* $K \in \mathbb{R}^{|\mathsf{F}|}$ as

$$K_{\mathsf{f}} \coloneqq \frac{1}{A_{\mathsf{f}}} \left(\sum_{\mathsf{p}\prec\mathsf{f}} \tilde{\angle}_{\mathsf{p},\mathsf{f}} - \pi \right). \tag{60}$$

On a closed surface, $(K_{\mathsf{f}})_{\mathsf{f}\in\mathsf{F}}$ satisfies the discrete Gauss–Bonnet theorem $\sum_{\mathsf{f}} A_{\mathsf{f}} K_{\mathsf{f}} = 2\pi\chi(M)$, where $\chi(M) = |\mathsf{P}| - |\mathsf{E}| + |\mathsf{F}|$ is the Euler characteristic.

To define the *discrete Gauss–Bonnet curvature* K_{f}^{Ω} (*cf.* (3.2)) we must incorporate the geodesic curvature into K_{f}. We do so by introducing another rescaled angle similar to (59) but this time also rescales the boundary angles:

$$\tilde{\angle}_{\mathsf{p},\mathsf{f}}^{\Omega} \coloneqq \begin{cases} \frac{2\pi}{\sum_{\mathsf{f}'\succ\mathsf{p}} \angle_{\mathsf{p},\mathsf{f}'}} \angle_{\mathsf{p},\mathsf{f}} & \text{for } \mathsf{p} \in \mathsf{I} \\ \frac{\pi}{\sum_{\mathsf{f}'\succ\mathsf{p}} \angle_{\mathsf{p},\mathsf{f}'}} \angle_{\mathsf{p},\mathsf{f}} & \text{for } \mathsf{p} \in \mathsf{B}. \end{cases} \tag{61}$$

Define the discrete Gauss–Bonnet curvature at face f as

$$K_{\mathsf{f}}^{\Omega} \coloneqq \frac{1}{A_{\mathsf{f}}} \left(\sum_{\mathsf{p}\prec\mathsf{f}} \tilde{\angle}_{\mathsf{p},\mathsf{f}}^{\Omega} - \pi \right). \tag{62}$$

When the surface has no boundary, $K_{\mathsf{f}}^{\Omega} = K_{\mathsf{f}}$. In general, these curvatures satisfy the discrete Gauss–Bonnet theorem with boundary: $\sum_{\mathsf{f}} A_{\mathsf{f}} K_{\mathsf{f}}^{\Omega} = 2\pi\chi(M)$.

5.2 Main Algorithm with the Free-Slip Condition

We now discretize the system (38) governing the vorticity field $w \in \mathbb{R}^{|\mathsf{P}|}$ and the coefficient tuple $\mathbf{c} = (c_i)_{i=1}^m \in \mathbb{R}^m$. In this section, we assume the free-slip boundary condition (Section 3.1). Specifically, we discretize system (45). The modification into other boundary conditions is detailed in Section 5.3.

Since the vorticity vanishes on the boundary following the formulation of (45), we have $w_{\mathsf{B}} = 0$. Thus, the fluid state is reduced to an *interior* vorticity field $w_{\mathsf{I}} \in \mathbb{R}^{|\mathsf{I}|}$ and $\mathbf{c} \in \mathbb{R}^m$. Given a precomputed L^2-orthonormal harmonic basis $(\mathbf{h}_i)_{i=1}^m$ with $\mathbf{h}_i \in \Gamma_{\mathsf{F}}(TM)$, the corresponding velocity field $\mathbf{u} \in \Gamma_{\mathsf{F}}(TM)$ is obtained by solving the Poisson problem (32) followed by the reconstruction step (31), using the discrete operators introduced in Section 5.1. We denote this process as $\mathbf{u} = \textsc{Velocity}(w_{\mathsf{I}}, \mathbf{c}; \mathbf{h})$:

$$\textsc{Velocity}(\cdot,\cdot;\mathbf{h}) : \mathbb{R}^{|\mathsf{I}|} \times \mathbb{R}^m \to \Gamma_{\mathsf{F}}(TM) \tag{63a}$$

$$\textsc{Velocity}(w_{\mathsf{I}}, \mathbf{c}; \mathbf{h}) \coloneqq -J \operatorname{grad} \psi + \textstyle\sum_{i=1}^m c_i \mathbf{h}_i \tag{63b}$$

$$\text{where} \quad L_{\mathsf{II}}\psi_{\mathsf{I}} = (A_{\mathsf{P}})_{\mathsf{II}} w_{\mathsf{I}}, \quad \psi_{\mathsf{B}} \equiv 0. \tag{63c}$$

Using this velocity and the discrete operators and curvature defined in Section 5.1, the system (45) translates into the following semi-discrete form:

$$\frac{d}{dt} w_{\mathsf{I}} = \overbrace{-[\nabla_{\mathbf{u}}]_{(\mathsf{I},:)} w}^{\textsc{Advect}(\mathbf{u},w)} + \overbrace{\nu \Delta_{(\mathsf{I},:)} w + 2\nu \operatorname{curl}_{(\mathsf{I},:)}((K_{\mathsf{f}}^{\Omega}\mathbf{u}_{\mathsf{f}})_{\mathsf{f}\in\mathsf{F}})}^{\textsc{Diffuse}(\mathbf{u},w)}, \tag{64a}$$

$$\frac{d}{dt} c_i = \underbrace{\textstyle\sum_{\mathsf{f}\in\mathsf{F}} A_{\mathsf{f}} \left(-w_{\mathsf{f}} \langle J_{\mathsf{f}}\mathbf{u}_{\mathsf{f}}, \mathbf{h}_{i,\mathsf{f}} \rangle + 2\nu K_{\mathsf{f}}^{\Omega} \langle \mathbf{u}_{\mathsf{f}}, \mathbf{h}_{i,\mathsf{f}} \rangle \right)}_{\textsc{HarmonicRate}(\mathbf{u},w)}, \tag{64b}$$

where $w_{\mathsf{f}} = \frac{1}{3} \sum_{\mathsf{p}\prec\mathsf{f}} w_{\mathsf{p}}$ is the vorticity field interpolated to the face, and w_{B} is kept zero.

We use an IMEX scheme (Algorithm 1) to integrate (64) in time, treating the nonstiff terms—namely $\textsc{Advect}(\mathbf{u}, w)$ in (64a) and $\textsc{HarmonicRate}(\mathbf{u}, w)$ of (64b) (*cf.* EvalRHS in Alg. 1)—with an explicit fourth-order Runge–Kutta method (*cf.* RK4Step), and the stiff term $\textsc{Diffuse}(\mathbf{u}, w)$ with an implicit Euler method: given $w_{\mathsf{I}}^{\text{old}}$ at the previous time step, solve the the vorticity $w_{\mathsf{I}}^{\text{new}}$ at the end of the time interval satisfying

$$w_{\mathsf{I}}^{\text{new}} - w_{\mathsf{I}}^{\text{old}} = \Delta t \, \textsc{Diffuse}(\mathbf{u}^{\text{new}}, w^{\text{new}}). \tag{65}$$

This is equivalent to

$$(A_{\mathsf{P}} + \nu \Delta t L)_{\mathsf{II}} w_{\mathsf{I}}^{\text{new}} = (A_{\mathsf{P}})_{\mathsf{II}} (w_{\mathsf{I}}^{\text{old}} + 2\nu \Delta t \operatorname{curl}_{(\mathsf{I},:)} (K^{\Omega} \mathbf{u}^{\text{new}})) \quad (66)$$

which can be solved by a fixed-point iteration (*cf.* FixedPoint). This fixed-point iteration typically converges in 2–3 iterations with tolerance $\varepsilon = 10^{-5}$.

Algorithm 1 IMEX Scheme for (45)

$\mathbf{h} = (\mathbf{h}_i)_{i=1}^{m} \leftarrow$ An orthonormal basis for $\mathfrak{H}$;
$w = (w_{\mathsf{p}})_{\mathsf{p} \in \mathsf{P}} \leftarrow$ Initialize vorticity; $w_{\mathsf{B}} \leftarrow 0$;
$\mathbf{c} = (c_i)_{i=1}^{m} \leftarrow$ Initialize harmonic coefficients;
$\Delta t > 0 \leftarrow$ Set time step;
tol $> 0 \leftarrow$ Set fixed-point iteration tolerance;
for each frame **do**
  $\begin{bmatrix} w_{\mathsf{I}} \\ \mathbf{c} \end{bmatrix} \leftarrow$ RK4Step (EvalRHS, $\begin{bmatrix} w_{\mathsf{I}} \\ \mathbf{c} \end{bmatrix}, \Delta t$) ; ▷ explicit step
  $w_{\mathsf{I}} \leftarrow$ FixedPoint $(w_{\mathsf{I}}, \mathbf{c}, \Delta t, \text{tol})$; ▷ implicit step
  export Velocity $(w_{\mathsf{I}}, \mathbf{c}; \mathbf{h})$;
function EvalRHS$(w_{\mathsf{I}}, \mathbf{c})$
  $\mathbf{u} \leftarrow$ Velocity $(w_{\mathsf{I}}, \mathbf{c}; \mathbf{h})$; ▷ *cf.* (63)
  $\dot{w}_{\mathsf{I}} \leftarrow$ Advect$(\mathbf{u}, w)$; ▷ *cf.* (64a)
  $\dot{\mathbf{c}} \leftarrow$ HarmonicRate$(\mathbf{u}, w)$; ▷ *cf.* (64b)
  return $(\dot{w}_{\mathsf{I}}, \dot{\mathbf{c}})$;
function FixedPoint$(w_{\mathsf{I}}, \mathbf{c}, \Delta t, \text{tol})$
  $w_{\mathsf{I}}^{\text{old}} \leftarrow w_{\mathsf{I}}$;
  do ▷ *cf.* (65)
    $\mathbf{u} \leftarrow$ Velocity $(w_{\mathsf{I}}, \mathbf{c}; \mathbf{h})$;
    $\tilde{w}_{\mathsf{I}} \leftarrow w_{\mathsf{I}}^{\text{old}} + 2\nu \Delta t \operatorname{curl}_{(\mathsf{I},:)} (K^{\Omega} \mathbf{u})$;
    $\tilde{w}_{\mathsf{I}} \leftarrow (A_{\mathsf{P}} + \nu \Delta t\, L)_{\mathsf{II}}^{-1} (A_{\mathsf{P}})_{\mathsf{II}} \tilde{w}_{\mathsf{I}}$;
    $\varepsilon \leftarrow \|\tilde{w} - w\|$; $w \leftarrow \tilde{w}$;
  while $\varepsilon >$ tol
  return w_{I};
function RK4Step$(F \in (\mathbb{T} \to \mathbb{T}), x \in \mathbb{T}, \Delta t \in \mathbb{R})$
  $k_1 \leftarrow F(x)$; $k_2 \leftarrow F(x + \Delta t/2 \cdot k_1)$;
  $k_3 \leftarrow F(x + \Delta t/2 \cdot k_2)$; $k_4 \leftarrow F(x + \Delta t \cdot k_3)$;
  return $x + \Delta t/6 \cdot (k_1 + 2k_2 + 2k_3 + k_4)$;

5.3 Friction and No-Slip Boundary Conditions

Algorithm 1 is a solver for fluids on closed surfaces or surfaces with free-slip boundary. We now describe its modifications into having friction boundary and no-slip boundary.

5.3.1 Navier Friction Boundary. As in the continuous theory (Section 3.2), adding friction amounts to modifying the Gauss–Bonnet curvature at the boundary (see (49) and (50)).

Continuing the definition of discrete Gauss–Bonnet curvature in Section 5.1.3, we introduce the rescaled angle that incorporate friction (*cf.* (61)):

$$\tilde{\angle}_{\mathsf{p},\mathsf{f}}^{\Omega,\alpha/(4\nu)} \coloneqq \frac{\pi}{(\sum_{\mathsf{f} \succ \mathsf{p}} \angle_{\mathsf{p},\mathsf{f}}) + \frac{\alpha}{4\nu} \ell_{\mathsf{p}}} \angle_{\mathsf{p},\mathsf{f}} \quad \text{for } \mathsf{p} \in \mathsf{B} \quad (67)$$

where ℓ_{p} is the averaged boundary edge length at vertex $\mathsf{p} \in \mathsf{B}$. For interior vertices $\mathsf{p} \in \mathsf{I}$, there is no modification: $\tilde{\angle}_{\mathsf{p},\mathsf{f}}^{\Omega,\alpha/(4\nu)} = \tilde{\angle}_{\mathsf{p},\mathsf{f}}^{\Omega}$. Define the *discrete Gauss–Bonnet curvature with friction* $\frac{\alpha}{4\nu}$:

$$K_{\mathsf{f}}^{\Omega,\alpha/(4\nu)} \coloneqq \frac{1}{A_{\mathsf{f}}} \left(\sum_{\mathsf{p} \prec \mathsf{f}} \tilde{\angle}_{\mathsf{p},\mathsf{f}}^{\Omega,\alpha/(4\nu)} - \pi \right). \quad (68)$$

To incorporate the friction boundary, the only algorithmic modification is replacing K^{Ω} by $K^{\Omega,\alpha/(4\nu)}$ in Algorithm 1.

Geometrically, this modification amounts to overwriting and inflating the value of the total interior angle of the boundary polygon $\sum_{\mathsf{f} \succ \mathsf{p}} \angle_{\mathsf{p},\mathsf{f}}$, and thereby decreasing the exterior angle echoing the expression $(\kappa_{\mathsf{g}} - \frac{\alpha}{4\nu})$ in (49). The net result decreases the rescaled angle $\tilde{\angle}$ at the boundary, introducing negative Gaussian curvature into the neighboring triangle.

The limiting case of infinity friction $\frac{\alpha}{4\nu} \to \infty$ corresponds to setting the rescaled angle to zero:

$$\tilde{\angle}_{\mathsf{p},\mathsf{f}}^{\Omega,\infty} = 0 \quad \text{for } \mathsf{p} \in \mathsf{B}. \quad (69)$$

5.3.2 No-Slip Boundary. One way to approximate the no-slip boundary condition is to apply the friction boundary (Section 5.3.1) with infinite friction coefficient, *i.e.* setting the rescaled angle to zero (69).

Alternatively, we impose the condition $u_{\partial} = 0$ by introducing a non-zero boundary vorticity w_{B} as in the description in Section 3.3.

For this latter setting, the system equation is reverted to (38) with a nonzero w_{B}. In particular, the Gaussian curvature K_{f}^{Ω} is replaced by K_{f} (given by (60)), that is, without the curvature sheet from the boundary. Note that with a non-zero w_{B}, a boundary contribution $\sum_{\mathsf{e} \in \partial M} \nu \langle (\mathbf{h}_i)_{\mathsf{f} \succ \mathsf{e}}, \mathbf{e}_{\mathsf{e}} \rangle w_{\mathsf{e}} \ell_{\mathsf{e}}$ need to be added in (64b). Here, $\mathbf{e}_{\mathsf{e}}$ is the unit edge direction and ℓ_{e} the edge length of edge e, and $w_{\mathsf{e}} = \sum_{\mathsf{p} \prec \mathsf{e}} \frac{w_{\mathsf{p}}}{2}$ for $\mathsf{p} \in \mathsf{B}$ denotes the vorticity field interpolated to the boundary edge.

The boundary vorticity field w_{B} is chosen to ensure that the boundary velocity

$$(u_{\partial})_{\mathsf{e}} = \langle \mathbf{u}_{\mathsf{f} \succ \mathsf{e}}, \mathbf{e}_{\mathsf{e}} \rangle \quad (70)$$

vanishes at each boundary edge $\mathsf{e} \in \partial M$ (*cf.* Section 3.3). This condition is enforced through a modified fixed-point iteration (Alg. 2).

Algorithm 2 Fixed-Point Iteration for No-Slip Boundary Condition

function FixedPointNoSlip$(w, \mathbf{c} = \{c_i\}, \Delta t, \text{tol}_w, \text{tol}_u, \beta)$
  $w^{\text{old}} \leftarrow w, \mathbf{c}^{\text{old}} \leftarrow \mathbf{c}$;
  do
    $\mathbf{u} \leftarrow$ Velocity $(w_{\mathsf{I}}, \mathbf{c}; \mathbf{h})$;
    $\tilde{w}_{\mathsf{I}} \leftarrow w_{\mathsf{I}}^{\text{old}} + 2\nu \Delta t (\operatorname{curl}(K\mathbf{u}))_{\mathsf{I}}$;
    $\tilde{w}_{\mathsf{B}} \leftarrow \tilde{w}_{\mathsf{B}} + \beta (u_{\partial})_{\mathsf{B}}$ ▷ $(u_{\partial})_{\mathsf{B}} \coloneqq$ (70) averaged to vertex
    $\tilde{w}_{\mathsf{I}} \leftarrow M_{\mathsf{II}}^{-1} ((A_{\mathsf{P}} \tilde{w})_{\mathsf{I}} - M_{\mathsf{IB}} \tilde{w}_{\mathsf{B}}), \quad M \coloneqq A_{\mathsf{P}} + \nu \Delta t L$;
    $\tilde{c}_i \leftarrow \tilde{c}_i^{\text{old}} + \Delta t \sum_{\mathsf{e} \in \partial M} \nu \langle (\mathbf{h}_i)_{\mathsf{f} \succ \mathsf{e}}, \mathbf{e}_{\mathsf{e}} \rangle \tilde{w}_{\partial,\mathsf{e}} \ell_{\mathsf{e}}$;
    $\varepsilon_w \leftarrow \|\tilde{w} - w\|$; $w \leftarrow \tilde{w}$;
    $\varepsilon_{\mathbf{c}} \leftarrow \|\tilde{\mathbf{c}} - \mathbf{c}\|$; $\mathbf{c} \leftarrow \tilde{\mathbf{c}}$;
  while $\varepsilon_w > \text{tol}_w$ **or** $\varepsilon_{\mathbf{c}} > \text{tol}_{\mathbf{c}}$ **or** $\|u_{\partial}\| > \text{tol}_u$
  return w;

The relaxation parameter $\beta > 0$ is chosen such that $\beta \ell_{\mathsf{p}} \approx 1$, where ℓ_{p} is the averaged edge length at p.

High-friction v.s. no-slip. As we will demonstrate in Figure 16, the high-friction boundary (Algorithm 1 with (69)) and the no-slip boundary (Algorithm 2) produce similar fluid-dynamical outcomes. However, the high-friction boundary treatment is significantly more efficient. The fixed-point iteration in Algorithm 1 remains robust even under infinite friction, whereas the fixed-point iteration in Algorithm 2 can become unstable at large Reynolds numbers, which can be mitigated by having higher resolution near the boundary.

6 NUMERICAL EXAMPLES

Our computation is implemented in SideFX Houdini. These tests were conducted on a Dell 8940 Desktop equipped with an Intel CPU i9-11900K operating at 3.50 GHz, 64 GB of RAM. For typical meshes—such as the example shown in Figure 15 with approximately 22K vertices— under free-slip or friction boundary conditions, the simulation using Alg. 1 takes about 90 minutes in total (about 5 seconds per frame). For no-slip condition shown in Figure 6, which has 16K vertices, the computation takes about 27 minutes (about 6 seconds per frame) using Alg. 1 and Alg. 2.

6.1 Viscous Laplacian

A common treatment of viscous dissipative in surface vortex dynamics involves only the Laplace–Beltrami operator applied to the vorticity. That is, in this approach the vorticity equation is modeled as $\dot{w}+\nabla_{\mathbf{u}} w = \nu\Delta w$ [Ebin and Marsden 1970; Yaeger et al. 1986; Elcott et al. 2007; Azencot et al. 2014; Vanneste 2021; Tao et al. 2024], which is equivalent to replacing the viscous Laplacian (Definition 2.9) in the Navier–Stokes equation (20) with the Hodge-Laplacian (Definition 2.8).

Contrary to this standard approach, we demonstrate that the curvature-dependent term $2\nu\,\mathrm{curl}(K\mathbf{u})$ in our vorticity equation (28) is crucial for capturing the correct dynamical behavior of fluid flows on curved surfaces.

We compare our method with that of [Azencot et al. 2014], which is based on solving $\dot{w} + \nabla_{\mathbf{u}} w = \nu\Delta w$ without the curvature-dependent term. To isolate the effects of curvature and avoid dependency of boundaries and harmonic components, the comparisons are performed on topological spheres.

In Figure 9, the vorticity field is initialized on a round sphere to represent a rigid body rotation. In the absence of shear deformation in a rigid motion, viscous dissipation should not occur, and conservation of angular momentum implies that the fluid should maintain its rotation indefinitely. Our method correctly preserves this rigid motion. In contrast, the model $\dot{w} + \nabla_{\mathbf{u}} w = \nu\Delta w$ fails to do so: the velocity rapidly decays to zero. This behavior is expected, as the Laplace–Beltrami operator on a closed surface has only constant functions in its kernel. Since the vorticity on a closed surface has zero mean, the dissipative term in this model ultimately drives the vorticity to zero.

Figure 10 presents another comparison, this time on a surface of revolution with non-uniform curvature. The initial condition is again a rigid body rotation. Our method preserves this motion, while the previous method introduces a non-physical distortion in the flow and eventually decays to rest.

6.2 Harmonic Dynamics and Preservation of Killing Modes

We further demonstrate that the evolution for the harmonic component in (38) is essential for accurately simulating viscous flows on non-simply-connected surfaces.

In Figure 11, we initialize the vorticity field on a torus with $w = -\langle \mathbf{n}, \hat{\mathbf{y}}\rangle$ and $c_1 = c_2 = 0$ on a torus, where $\mathbf{n}$ is the surface normal, and $\hat{\mathbf{y}}$ is the upward-pointing unit vector. We compare the results of our full system (38), which includes harmonic evolution, against a version of the system with the harmonic dynamics disabled (*i.e.*, $\dot{\mathbf{c}} = \mathbf{0}$). At each time step, we extract both the harmonic component and the Killing component of the velocity field.

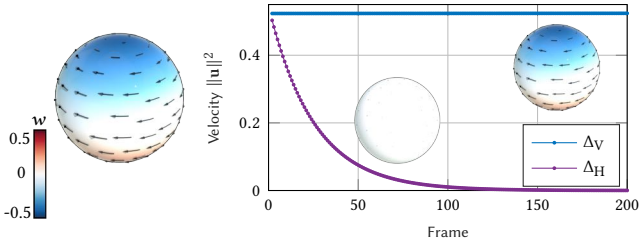

Fig. 9. Comparison of viscosity modeled using the viscous Laplacian Δ_V (our method) versus the Hodge Laplace Δ_H (previous methods). An initial rigid body rotation is preserved in our model. In contrast, the Hodge Laplacian model—corresponding to the vorticity equation $\dot{w} + \nabla_{\mathbf{u}} w = \nu\Delta w$—fails to preserve rigid body motion and instead dissipates it.

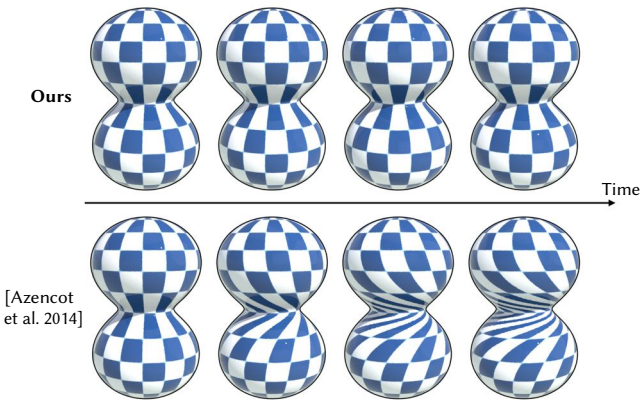

Fig. 10. Viscous flow on a surface of revolution with non-uniform curvature, initialized with a rigid body rotation. Our method correctly preserve the rigid body motion, and thus the advected textures, while previous vorticity methods using $\dot{w} + \nabla_{\mathbf{u}} w = \nu\Delta w$ produce non-physical distortions. The initial angular velocity is 1 and the viscosity is $\nu = 0.1$. The sequence shows frames 1, 30, 75, 150 with $\Delta t = 0.1$.

When the harmonic evolution is omitted, the Killing fields on the torus fail to be conserved, violating the conservation property stated in Theorem 2.2. In contrast, when the harmonic field dynamics are included, the Killing field component is successfully preserved. Interestingly, we also observe a nontrivial interchange between the harmonic component and the vorticity over time.

Figure 12 shows a simulation on an *Enneper surface*, which possesses an intrinsic Killing field that is not the restriction of a rigid body motion in $\mathbb{R}^3$. This surface has two boundaries, where we impose the free-slip boundary condition. Even in this more general setting, our method preserves the Killing mode, in agreement with Theorem 2.2. As in Figure 11, the initial condition is given by $w = -\langle \mathbf{n}, \hat{\mathbf{y}}\rangle$ and $c_1 = 0$. The flow relaxes to a pure Killing field.

6.3 Non-Orientatable surfaces

We demonstrate fluid simulation on non-orientable surfaces using our algorithm and the double cover technique in Section 4.

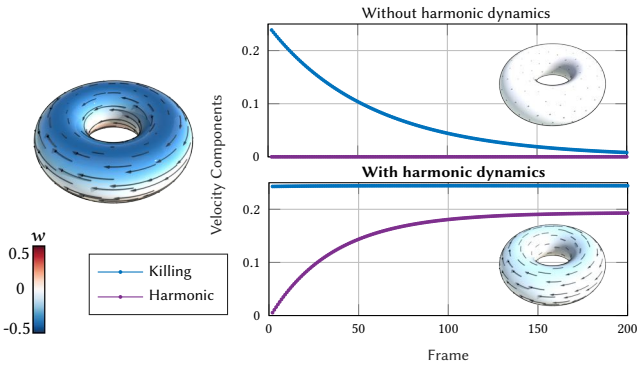

Fig. 11. Comparison of fluid dynamics on a torus using the full system (38) (bottom right), which includes harmonic component evolution, versus a system with harmonic dynamics disabled (top right), both initialized from the same initial condition (left). The plots show the evolution of the Killing field and harmonic field components over time. The full system preserves the Killing component and reveals interaction between the harmonic and vorticity components. In contrast, disabling the harmonic dynamics causes the Killing component to be incorrectly damped out. Here $\nu = 0.1, \Delta t = 0.1$.

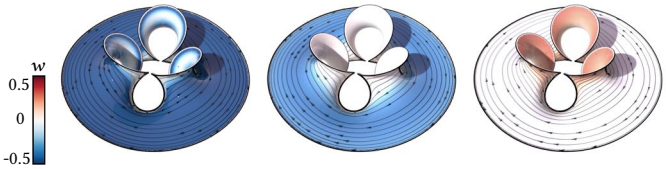

Fig. 12. Viscous flow simulated on an Enneper surface, which possesses an intrinsic Killing field. The free-slip condition is imposed at the boundary. An initial flow (left) relaxes to the pure Killing field (right). The viscosity is $\nu = 0.1$. The sequence shows frames 2, 50, 300 with $\Delta t = 0.1$.

Fig. 13. Kelvin–Helmholtz instability on a Möbius strip. The initial condition includes a vortex sheet along the boundary of the blue region and a nonzero harmonic component, forming a jet within the blue region. The Möbius strip has width 1, the initial jet speed is 0.1, the viscosity is $\nu = 10^{-5}$, and the time step is $\Delta t = 0.1$. The sequence shows frames 1, 600, 780.

The *Boy surface* shown in Figure 1 has the topology of $\mathbb{RP}^2$, whose oriented double cover is a topological sphere. The *Möbius strip* in Figure 13 is double-covered by a cylinder. The *Klein bottle* in Figure 14 is double-covered by a torus. The simulation runs on the oriented double covering mesh with an initial condition that obeys the even/odd parity in Table 1.

Fig. 14. Fluid simulation on a Klein bottle. The initial condition is set with a jet along the tube similar to that of Figure 13. The sequence shows frames 1, 50, 300.

6.4 Boundary Conditions

While the previous examples in Figures 5, 12, and 13 demonstrate the behavior of fluids under the free-slip boundary condition, we now examine the influence of friction applied at the boundary.

Figure 6 shows that the no-slip boundary condition on a moving boundary—enforced via Algorithm 2—can set motion in an initially stationary viscous fluid.

In Figure 15, a small disk is removed from a torus to represent a fluid obstacle. The initial condition is set with zero vorticity but a nonzero harmonic component, producing a background flow past the obstacle. When the obstacle boundary is set as free-slip (top row), a small amount of vorticity is generated, but insufficient to form a von Kármán vortex street. In contrast, when the boundary is given high friction—approximated by a near-infinite relative friction coefficient $\frac{\alpha}{4\nu} \gg 1$ to emulating a no-slip boundary (bottom row)—vortex shedding is significantly enhanced, resulting in the formation of a von Kármán vortex street.

Figure 16 compares two no-slip boundary treatments: one using a high-friction boundary, as in Figure 15 (bottom), and the other enforcing the hard no-slip constraint computed with Algorithm 2. While both approaches yield similar results, the high-friction method is significantly more efficient. Moreover, the fixed-point iteration in Algorithm 2 requires a finer mesh near the boundary to ensure convergence, which is the domain employed for Figure 16.

Figure 17 compares flow past a high-friction obstacle at two different viscosities, *i.e.*, two different Reynolds numbers. From both Figure 15 and Figure 17, one can observe that vorticity exhibits greater numerical dispersion (spatial oscillation) at higher Reynolds numbers and lower resolutions. Such dispersion is expected from the discrete operator (58) [Azencot et al. 2014]. Note, however, that these dispersive oscillations appear in the vorticity field (a derivative quantity) and have little effect on the velocity field (an integrated quantity) or on the resulting fluid animation.

Figure 18 presents a similar experiment conducted on the Klein bottle.

7 CONCLUSION

We have presented a vorticity formulation of the Navier–Stokes equations on general surfaces, along with a corresponding numerical

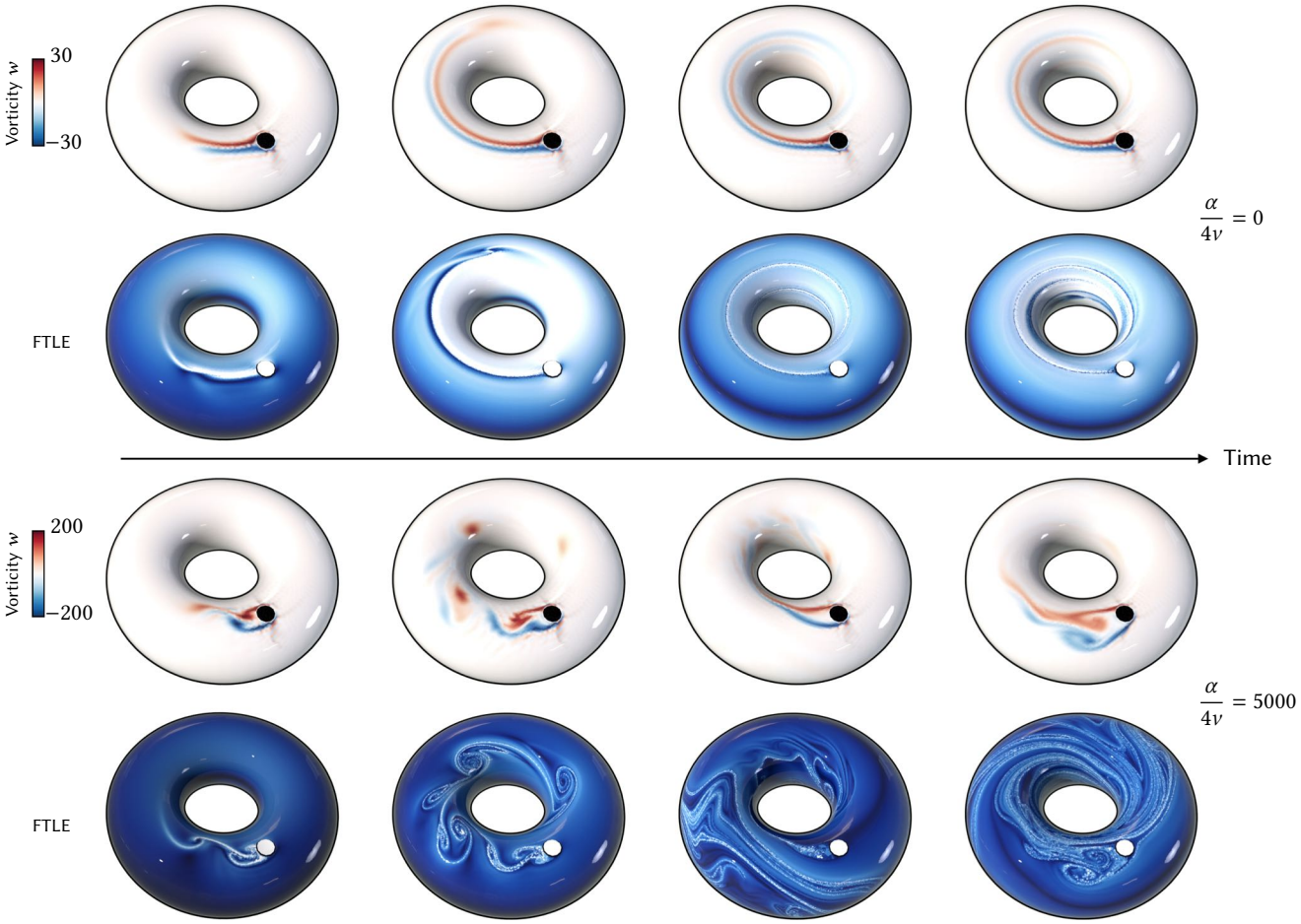

Fig. 15. Flow past an obstacle on a torus. With identical initial conditions and fluid viscosity, the relative friction coefficient at the boundary affects the extent of vortex shedding. Compared to the free-slip boundary (top row), the near-no-slip friction boundary (bottom row) produces pronounced vortex shedding, leading to the formation of a von Kármán vortex street. The flows are visualized using vorticity and the backward-time Finite-Time Lyapunov Exponent (FTLE) [Haller 2015]. The torus has radii 1 and 0.5; the initial harmonic component has $c = 10$; the viscosity is $\nu = 10^{-3}$; and the simulation uses $\Delta t = 0.002$. The sequence shows frames 61, 201, 751, 996.

algorithm. A central contribution is our emphasis on curvature-related terms in the viscous force, which influence both the vorticity equation and the evolution of harmonic components. By comparing our full model with commonly used simplified variants that omit curvature effects or harmonic dynamics, we demonstrate that only the complete system reproduces physically meaningful behavior, such as the conservation of frictionless rigid motions.

Our numerical scheme is conditionally stable, similar to the approaches in [Azencot et al. 2014] and [Yin et al. 2023], with the advection step subject to a CFL condition. The implicit treatment of the viscous force (Algorithm 1) and the no-slip condition (Algorithm 2) is carried out using fixed-point iterations. While fixed-point methods are simple to implement and converge quickly for the main algorithm (Algorithm 1), they are less efficient for enforcing the no-slip condition. We believe that Newton's method may be better suited for these implicit steps, and we leave its development for future work.

A notable analytical result of our study is an explicit formula for the jump condition of vorticity across a sheet of singular Gaussian curvature. This mathematical result is used to simplify the enforcement of boundary conditions: by interpreting boundary geodesic curvature, augmented by the friction coefficient, as a singular sheet of Gaussian curvature, the correct vorticity at the boundary naturally

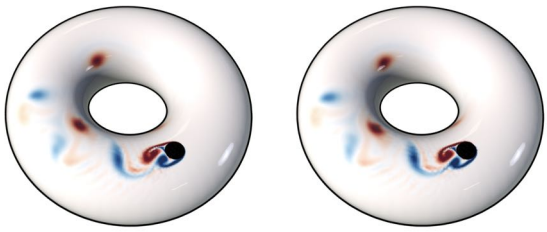

Fig. 16. Comparison between a high-friction boundary condition ($\frac{\alpha}{4\nu} = 1000$) (left) and the no-slip condition computed with Algorithm 2 (right). Producing similar results, the high-friction boundary is computationally more efficient. The mesh is refined near the boundary. Frame 201 is shown.

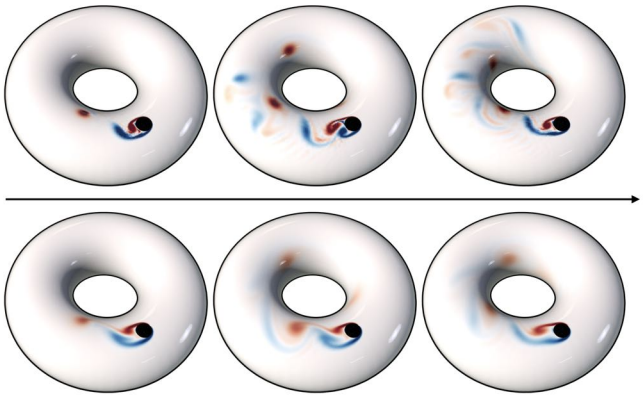

Fig. 17. Flow past a high-friction ($\frac{\alpha}{4\nu} = 1000$) obstacle on a torus with low viscosity ($\nu = 10^{-3}$, top) and high viscosity ($\nu = 10^{-2}$, bottom). Vortex shedding occurs in both cases, forming von Kármán vortex streets at two different Reynolds numbers. The sequence shows frames 61, 201, 301.

emerges through the jump condition. This approach is useful even in flat domains with curved boundaries.

Under free-slip boundary condition, our formulation of the harmonic evolution equation reveals a direct relationship between boundary curvature, boundary velocity, and the dynamics of harmonic components (Corollary 3.1). This observation may provide new mathematical insight into the Kutta condition and complements recent work aimed at developing its theoretical foundation [Taha et al. 2023].

Finally, we describe a general technique for simulating fluids on non-orientable surfaces by constructing their oriented double cover and carefully distinguishing between even and odd types of vector fields and differential forms. This approach, in particular, leads to a natural extension of the computational Hodge decomposition to non-orientable surfaces (Section 4.1.3).

We hope that these contributions will inspire further developments at the intersection of geometry and fluid dynamics.

ACKNOWLEDGMENTS

The work is supported by NSF CAREER Award 2239062. The authors thank Dr. Oliver Gross for the Enneper surface. Additional support is provided by the SideFX Software.

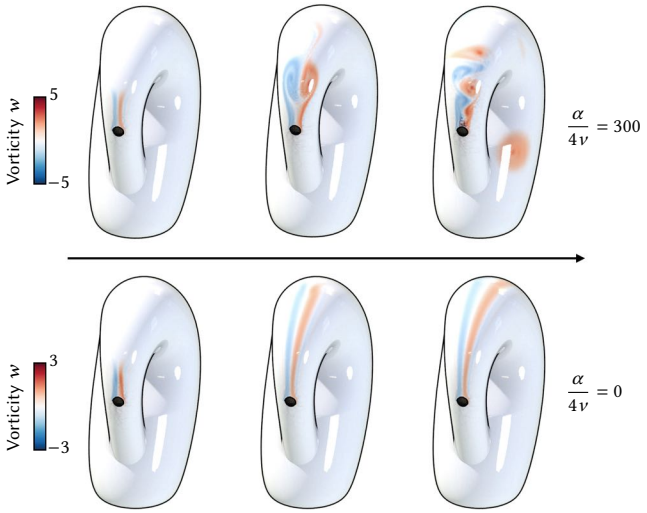

Fig. 18. Flow past an obstacle on a Klein bottle with identical initial conditions and viscosity. Top row: friction boundary condition produces a von Kármán vortex street. Bottom row: free-slip boundary condition. The initial harmonic component has $c = 0.5$, and the viscosity is $\nu = 10^{-5}$. The sequence shows frames 30, 160, 390.

REFERENCES

Christopher R Anderson. 1989. Vorticity boundary conditions and boundary vorticity generation for two-dimensional viscous incompressible flows. *J. Comput. Phys.* 80, 1 (1989), 72–97.

Omri Azencot, Steffen Weißmann, Maks Ovsjanikov, Max Wardetzky, and Mirela Ben-Chen. 2014. Functional fluids on surfaces. In *Computer Graphics Forum*, Vol. 33. Wiley Online Library, 237–246.

Mirela Ben-Chen, Adrian Butscher, Justin Solomon, and Leonidas Guibas. 2010. On discrete killing vector fields and patterns on surfaces. In *Computer Graphics Forum*, Vol. 29. Wiley Online Library, 1701–1711.

Leonardo Carvalho, Maria Andrade, and Luiz Velho. 2012. Fluid Simulation on Surfaces in the GPU. In *2012 25th SIBGRAPI Conference on Graphics, Patterns and Images*. IEEE, 205–212.

Chi Hin Chan, Magdalena Czubak, and Marcelo M Disconzi. 2017. The formulation of the Navier–Stokes equations on Riemannian manifolds. *Journal of Geometry and Physics* 121 (2017), 335–346.

Alexandre Joel Chorin. 1973. Numerical study of slightly viscous flow. *Journal of fluid mechanics* 57, 4 (1973), 785–796.

Alexandre Joel Chorin. 1978. Vortex sheet approximation of boundary layers. *Journal of computational physics* 27, 3 (1978), 428–442.

Alexandre Joel Chorin. 1980. Vortex models and boundary layer instability. *SIAM J. Sci. Statist. Comput.* 1, 1 (1980), 1–21.

GH Cottet. 2000. Vortex Methods: Theory and Practice.

G. H. Cottet. 1988. Vorticity boundary conditions and the deterministic vortex method for the Navier-Stokes equation. In *Mathematical Aspects of Vortex Dynamics*, Russel E. Caflish (Ed.). SIAM, 128–143.

Qiaodong Cui, Timothy Langlois, Pradeep Sen, and Theodore Kim. 2021. Spiral-spectral fluid simulation. *ACM Transactions on Graphics (TOG)* 40, 6 (2021), 202:1–202:16.

Georges De Rham. 1984. *Differentiable manifolds: forms, currents, harmonic forms*. Vol. 266. Springer Science & Business Media.

Weinan E and Jian-Guo Liu. 1996. Vorticity boundary condition and related issues for finite difference schemes. *Journal of computational physics* 124, 2 (1996), 368–382.

David G Ebin and Jerrold Marsden. 1970. Groups of diffeomorphisms and the motion of an incompressible fluid. *Annals of Mathematics* 92, 1 (1970), 102–163.

Sharif Elcott, Yiying Tong, Eva Kanso, Peter Schröder, and Mathieu Desbrun. 2007. Stable, circulation-preserving, simplicial fluids. *ACM Transactions on Graphics (TOG)* 26, 1 (2007), 4–es.

Philip M Gresho. 1991. Incompressible fluid dynamics: some fundamental formulation issues. *Annual review of fluid mechanics* 23 (1991), 413–453.

Ben J Gross, Nathaniel Trask, Paul Kuberry, and Paul J Atzberger. 2020. Meshfree methods on manifolds for hydrodynamic flows on curved surfaces: A Generalized

Moving Least-Squares (GMLS) approach. *J. Comput. Phys.* 409 (2020), 109340.
George Haller. 2015. Lagrangian coherent structures. *Annual review of fluid mechanics* 47, 1 (2015), 137–162.
Kyle Hegeman, Michael Ashikhmin, Hongyu Wang, Hong Qin, and Xianfeng Gu. 2009. GPU-based conformal flow on surfaces. *Commun. Inf. Syst* (2009).
David J Hill and Ronald D Henderson. 2016. Efficient fluid simulation on the surface of a sphere. *ACM Transactions on Graphics (TOG)* 35, 2 (2016), 1–9.
Weizhen Huang, Julian Iseringhausen, Tom Kneiphof, Ziyin Qu, Chenfanfu Jiang, and Matthias B Hullin. 2020. Chemomechanical simulation of soap film flow on spherical bubbles. *ACM Transactions on Graphics (TOG)* 39, 4 (2020), 41:1–41:13.
Sadashige Ishida, Peter Synak, Fumiya Narita, Toshiya Hachisuka, and Chris Wojtan. 2020. A model for soap film dynamics with evolving thickness. *ACM Transactions on Graphics (TOG)* 39, 4 (2020), 31:1–31:11.
James P Kelliher. 2006. Navier–Stokes equations with Navier boundary conditions for a bounded domain in the plane. *SIAM journal on mathematical analysis* 38, 1 (2006), 210–232.
SN Kempka, JH Strickland, MW Glass, JS Peery, and MS Ingber. 1995. *Velocity boundary conditions for vorticity formulations of the incompressible Navier-Stokes equations.* Technical Report. Sandia National Lab.(SNL-NM), Albuquerque, NM (United States).
Petros Koumoutsakos, Anthony Leonard, and F Pepin. 1994. Boundary conditions for viscous vortex methods. *J. Comput. Phys.* 113, 1 (1994), 52–61.
Michael James Lighthill. 1963. Introduction boundary layer theory. *Laminar boundary layers* (1963).
Ingo Nitschke, Sebastian Reuther, and Axel Voigt. 2017. Discrete exterior calculus (DEC) for the surface Navier-Stokes equation. *Transport processes at fluidic interfaces* (2017), 177–197.
Ingo Nitschke, Sebastian Reuther, and Axel Voigt. 2021. Vorticity-stream function approaches are inappropriate to solve the surface Navier-Stokes equation on a torus. *PAMM* 20, 1 (2021), e202000006.
Marcel Padilla. 2018. *Point vortex dynamics on closed surfaces.* Master's thesis. Technische Universität Berlin.
L Quartapelle. 1981. Vorticity conditioning in the computation of two-dimensional viscous flows. *J. Comput. Phys.* 40, 2 (1981), 453–477.
L Quartapelle and F Valz-Gris. 1981. Projection conditions on the vorticity in viscous incompressible flows. *International Journal for Numerical Methods in Fluids* 1, 2 (1981), 129–144.
Dietmar Rempfer. 2006. On boundary conditions for incompressible Navier-Stokes problems. (2006).
Patrick J Roache. 1976. *Computational Fluid Dynamics.* Hermosa Publishers.
Maryam Samavaki and Jukka Tuomela. 2020. Navier–Stokes equations on Riemannian manifolds. *Journal of Geometry and Physics* 148 (2020), 103543.
Lin Shi and Yizhou Yu. 2004. Inviscid and incompressible fluid simulation on triangle meshes. *Computer Animation and Virtual Worlds* 15, 3-4 (2004), 173–181.
Jos Stam. 2003. Flows on surfaces of arbitrary topology. *ACM Transactions On Graphics (TOG)* 22, 3 (2003), 724–731.
Haithem Taha, Cody Gonzalez, and Mohamed Shorbagy. 2023. A minimization principle for incompressible fluid mechanics. *Physics of Fluids* 35, 12 (2023).
Ningxiao Tao, Liangwang Ruan, Yitong Deng, Bo Zhu, Bin Wang, and Baoquan Chen. 2024. A Vortex Particle-on-Mesh Method for Soap Film Simulation. *ACM Transactions on Graphics (TOG)* 43, 4 (2024), 1–14.
Michael E Taylor et al. 1996. *Partial differential equations III* (3 ed.). Applied Mathematical Sciences, Vol. 117. Springer.
Alexander Thom. 1933. The flow past circular cylinders at low speeds. *Proceedings of the Royal Society of London. Series A, Containing Papers of a Mathematical and Physical Character* 141, 845 (1933), 651–669.
Jacques Vanneste. 2021. Vortex dynamics on a Möbius strip. *Journal of Fluid Mechanics* 923 (2021), A12.
Sinan Wang, Yitong Deng, Molin Deng, Hong-Xing Yu, Junwei Zhou, Duowen Chen, Taku Komura, Jiajun Wu, and Bo Zhu. 2024. An Eulerian Vortex Method on Flow Maps. *ACM Transactions on Graphics (TOG)* 43, 6 (2024), 1–14.
Larry Yaeger, Craig Upson, and Robert Myers. 1986. Combining physical and visual simulation—creation of the planet jupiter for the film "2010". *Acm Siggraph Computer Graphics* 20, 4 (1986), 85–93.
Bowen Yang, William Corse, Jiecong Lu, Joshuah Wolper, and Chen-Fanfu Jiang. 2019. Real-time fluid simulation on the surface of a sphere. *Proceedings of the ACM on Computer Graphics and Interactive Techniques* 2, 1 (2019), 1–17.
Hang Yin, Mohammad Sina Nabizadeh, Baichuan Wu, Stephanie Wang, and Albert Chern. 2023. Fluid Cohomology. *ACM Trans. Graph.* 42, 4, Article 126 (July 2023), 25 pages. https://doi.org/10.1145/3592402

A KILLING OPERATOR

This appendix elaborates on the Killing operator (Definition 2.1) and provides proofs for Propositions 2.1, 2.2, 3.1, and Theorems 2.1, 2.2.

The proofs of Proposition 2.1 and Theorem 2.2 rely only on elementary differential geometry and are presented in Appendix A.1 and Appendix A.2, respectively.

In contrast, the proofs of Propositions 2.2, 3.1, and Theorem 2.1 become significantly simpler once we establish the relationship between the Killing operator and the *Dolbeault operator* $\bar{\partial}$, under the identification of the tangent bundle TM as a *complex line bundle*, as explained in Appendix A.3.

A.1 Proof of Proposition 2.1

We show that $(\mathcal{K}\mathbf{u})[\![\mathbf{a},\mathbf{b}]\!] = \frac{1}{2}(\langle\nabla_{\mathbf{a}}\mathbf{u},\mathbf{b}\rangle + \langle\nabla_{\mathbf{b}}\mathbf{u},\mathbf{a}\rangle)$, where $\mathcal{K}\mathbf{u} \coloneqq \frac{1}{2}\mathcal{L}_{\mathbf{u}}\, g$.

Apply the product rule for Lie derivative:

$$\mathcal{L}_{\mathbf{u}}(g[\![\mathbf{a},\mathbf{b}]\!]) = (\mathcal{L}_{\mathbf{u}}\, g)[\![\mathbf{a},\mathbf{b}]\!] + g[\![\mathcal{L}_{\mathbf{u}}\,\mathbf{a},\mathbf{b}]\!] + g[\![\mathbf{a},\mathcal{L}_{\mathbf{u}}\,\mathbf{b}]\!]. \tag{71}$$

Express the metric as $g[\![\cdot,\cdot]\!] = \langle\cdot,\cdot\rangle$, and use the identity $\mathcal{L}_{\mathbf{u}}\,\mathbf{a} = [\mathbf{u},\mathbf{a}] = \nabla_{\mathbf{u}}\mathbf{a} - \nabla_{\mathbf{a}}\mathbf{u}$, which holds because the Levi-Civita connection ∇ is torsion-free. The left-hand side of (71) becomes

$$\mathcal{L}_{\mathbf{u}}\langle\mathbf{a},\mathbf{b}\rangle = d_{\mathbf{u}}\langle\mathbf{a},\mathbf{b}\rangle = \langle\nabla_{\mathbf{u}}\mathbf{a},\mathbf{b}\rangle + \langle\mathbf{a},\nabla_{\mathbf{u}}\mathbf{b}\rangle, \tag{72}$$

by metric compatibility of ∇. Substituting this into (71), we get:

$$\begin{aligned}\cancel{\langle\nabla_{\mathbf{u}}\mathbf{a},\mathbf{b}\rangle} + \cancel{\langle\mathbf{a},\nabla_{\mathbf{u}}\mathbf{b}\rangle} = 2(\mathcal{K}\mathbf{u})[\![\mathbf{a},\mathbf{b}]\!] &+ \cancel{\langle\nabla_{\mathbf{u}}\mathbf{a}} - \nabla_{\mathbf{a}}\mathbf{u},\mathbf{b}\rangle \\ &+ \langle\mathbf{a},\cancel{\nabla_{\mathbf{u}}\mathbf{b}} - \nabla_{\mathbf{b}}\mathbf{u}\rangle,\end{aligned} \tag{73}$$

which implies the desired identity (6). □

A.2 Proof of Theorem 2.2

We show that the component of the velocity field along a Killing vector field is conserved under the Navier–Stokes equation.

Let $\mathbf{v} \in \ker(\mathcal{K})$ be a Killing vector field. By Proposition 2.1, it satisfies the identity

$$\langle\nabla_{\mathbf{a}}\mathbf{v},\mathbf{b}\rangle = -\langle\nabla_{\mathbf{b}}\mathbf{v},\mathbf{a}\rangle. \tag{74}$$

Suppose the velocity field $\mathbf{u}$ satisfies the Navier–Stokes equation (20): $\dot{\mathbf{u}} + \nabla_{\mathbf{u}}\mathbf{u} = -\operatorname{grad} p + \nu\Delta_{\mathrm{V}}\mathbf{u}$. We take the L^2 inner product of both sides of the equation with the Killing field $\mathbf{v}$. The first term yields $\langle\!\langle\dot{\mathbf{u}},\mathbf{v}\rangle\!\rangle = \frac{d}{dt}\langle\!\langle\mathbf{u},\mathbf{v}\rangle\!\rangle$, which is the time derivative of the projection of $\mathbf{u}$ onto the Killing field $\mathbf{v}$. Our goal is to show that the remaining terms $\langle\!\langle -\nabla_{\mathbf{u}}\mathbf{u} - \operatorname{grad} p + \nu\Delta_{\mathrm{V}}\mathbf{u},\mathbf{v}\rangle\!\rangle$ vanish, thus establishing $\frac{d}{dt}\langle\!\langle\mathbf{u},\mathbf{v}\rangle\!\rangle = 0$.

We first observe that $\langle\!\langle\Delta_{\mathrm{V}}\mathbf{u},\mathbf{v}\rangle\!\rangle = 0$. This follows from the fact that Δ_{V} is the functional gradient of $\mathcal{E}_{\mathrm{V}}[\mathbf{u}] = \|\mathcal{K}\mathbf{u}\|^2$ (Definition 2.6), and hence[8] $\langle\!\langle\Delta_{\mathrm{V}}\mathbf{u},\mathbf{v}\rangle\!\rangle = 2\langle\!\langle\mathcal{K}\mathbf{u},\mathcal{K}\mathbf{v}\rangle\!\rangle = 0$ (since $\mathcal{K}\mathbf{v} = 0$).

Next, we have $\langle\!\langle -\operatorname{grad} p,\mathbf{v}\rangle\!\rangle = \langle\!\langle p,\operatorname{div}\mathbf{v}\rangle\!\rangle = 0$, since every Killing field is divergence-free.

It remains to show that $\langle\!\langle\nabla_{\mathbf{u}}\mathbf{u},\mathbf{v}\rangle\!\rangle = 0$. Using integration by parts and the divergence-freeness of $\mathbf{u}$, we have $\langle\!\langle\nabla_{\mathbf{u}}\mathbf{u},\mathbf{v}\rangle\!\rangle = -\langle\!\langle\mathbf{u},\nabla_{\mathbf{u}}\mathbf{v}\rangle\!\rangle$, which vanishes by the skew-symmetry of $\nabla\mathbf{v}$ in (74). □

A.3 Killing Operator in terms of Complex Analysis on Complex Manifolds

For an oriented compact Riemannian 2-manifold M, the tangent bundle TM, equipped with the counterclockwise 90° rotation operator J, becomes a *complex line bundle* over M. This complex structure

[8] If $\partial M \neq \emptyset$, the natural boundary condition (*i.e.*, the free-slip condition from Proposition 3.1) must be imposed on $\mathbf{u}$.

endows M with the structure of a *Riemann surface*. Compact Riemann surfaces are, in fact, *complex algebraic curves*, and as such, they naturally admit several important operators from complex analysis, which we now introduce.

A.3.1 Complex-Linear and Anti-Linear Forms. The complex structure J on TM induces a corresponding complex structure on 1-forms, represented by the Hodge star operator $\star_1$ acting on 1-forms. This operator is related to J by the adjoint relation:

$$\langle \alpha | J\mathbf{a} \rangle = \langle - \star_1 \alpha | \mathbf{a} \rangle, \quad \alpha \in \Omega^1(M), \mathbf{a} \in \Gamma(TM). \tag{75}$$

Equivalently, this means $- \star_1 \alpha = \alpha \circ J$.

For brevity, we will omit the subscript k in the Hodge star $\star_k$ acting on k-forms, unless needed for clarity.

With both TM and T^*M now endowed with complex structures, we can classify vector-valued 1-forms according to whether they preserve or reverse the complex structure.

Definition A.1. *A vector-valued 1-form $A \in \Omega^1(M, TM)$ is said to be:*

- ***complex-linear*** *if $- \star A = A \circ J = J \circ A$.*
- ***complex-antilinear*** *if $- \star A = A \circ J = -J \circ A$.*

The corresponding spaces of complex-(anti)linear vector-valued 1-forms are:

$$\Gamma(K \otimes TM) \coloneqq \{A \in \Omega^1(M, TM) \mid - \star A = JA\} \tag{76}$$

$$\Gamma(\overline{K} \otimes TM) \coloneqq \{A \in \Omega^1(M, TM) \mid \star A = JA\} \tag{77}$$

Here, K denotes the *canonical bundle* of the algebraic curve M.

Every vector-valued 1-form admits a decomposition into complex-linear and a complex-antilinear components:

$$\Omega^1(M, TM) = \Gamma(K \otimes TM) \oplus \Gamma(\overline{K} \otimes TM), \tag{78a}$$

$$A = \underbrace{\tfrac{1}{2}(A + J \star A)}_{\in \Gamma(K \otimes TM)} + \underbrace{\tfrac{1}{2}(A - J \star A)}_{\in \Gamma(\overline{K} \otimes TM)}. \tag{78b}$$

These two componets are orthogonal under the Frobenius product:

$$\langle A \wedge \star B \rangle = 0 \quad \forall\, A \in \Gamma(K \otimes TM), B \in \Gamma(\overline{K} \otimes TM). \tag{79}$$

The complex-linear and complex-antilinear tensors can also be understood in terms of symmetric and skew-symmetric bilinear forms. Applying the $\flat$ operator to a vector-valued 1-form yields a covector-valued 1-form, (*i.e.*, a bilinear form), defined by

$$A^\flat [\![\mathbf{a}, \mathbf{b}]\!] \coloneqq \langle A\mathbf{a}, \mathbf{b} \rangle. \tag{80}$$

One can vertify that

$$A \in \Gamma(\overline{K} \otimes TM) \text{ if and only if } A^\flat \text{ is symmetric and } \operatorname{tr}(A) = 0. \tag{81}$$

In fact, the complex-linear part $A' \coloneqq \frac{1}{2}(A + J \star A)$ and the complex-antilinear part $A'' \coloneqq \frac{1}{2}(A - J \star A)$ correspond respectively to the trace/skew-symmetric part and the trace-free symmetric part of $A^\flat$:

$$(A')^\flat [\![\mathbf{a}, \mathbf{b}]\!] = \tfrac{1}{2} \operatorname{tr}(A) \langle \mathbf{a}, \mathbf{b} \rangle + \tfrac{1}{2}(\langle A\mathbf{a}, \mathbf{b} \rangle - \langle A\mathbf{b}, \mathbf{a} \rangle), \tag{82a}$$

$$(A'')^\flat [\![\mathbf{a}, \mathbf{b}]\!] = \tfrac{1}{2}(\langle A\mathbf{a}, \mathbf{b} \rangle + \langle A\mathbf{b}, \mathbf{a} \rangle) - \tfrac{1}{2} \operatorname{tr}(A) \langle \mathbf{a}, \mathbf{b} \rangle. \tag{82b}$$

These expressions can be verified by evaluating on vectors from a (pointwise) orthonormal basis.

A.3.2 Decomposition of Vector Gradients. Vector-valued 1-forms are fundamental objects in the analysis of flow fields, as they naturally arise when differentiating a vector field such as the velocity. Specifically, the Levi-Civita covariant derivative of a vector field $\mathbf{u} \in \Gamma(TM)$ is a vector-valued 1-form $\nabla \mathbf{u} \in \Omega^1(M, TM)$.

Applying the decomposition from (78) to $\nabla \mathbf{u}$, we obtain its complex-linear and complex-antilinear components, denoted by $\partial \mathbf{u}$ and $\bar{\partial} \mathbf{u}$ respectively.

Definition A.2. *The **Wirtinger differential operators** $\partial \colon \Gamma(TM) \to \Gamma(K \otimes TM)$ and $\bar{\partial} \colon \Gamma(TM) \to \Gamma(\overline{K} \otimes TM)$ (the latter also known as the **Dolbeault operator**) are defined as*

$$\partial \mathbf{u} \coloneqq \tfrac{1}{2}(\nabla \mathbf{u} + J \star \nabla \mathbf{u}) \tag{83}$$

$$\bar{\partial} \mathbf{u} \coloneqq \tfrac{1}{2}(\nabla \mathbf{u} - J \star \nabla \mathbf{u}), \tag{84}$$

which are the complex-linear and complex-antilinear parts of $\nabla \mathbf{u}$:

$$\nabla \mathbf{u} = \partial \mathbf{u} + \bar{\partial} \mathbf{u}. \tag{85}$$

By (82), Proposition 2.1, the fact that $\operatorname{tr}(\nabla \mathbf{u}) = \operatorname{div}(\mathbf{u})$, and the fact that $d(\mathbf{u}^\flat)$ corresponds to twice the skew-symmetric part[9] of $\nabla \mathbf{u}$, we obtain:

$$(\partial \mathbf{u})^\flat = \tfrac{1}{2}(\operatorname{div} \mathbf{u}) g + \tfrac{1}{2} d(\mathbf{u}^\flat) \tag{86}$$

$$(\bar{\partial} \mathbf{u})^\flat = \mathcal{K}\mathbf{u} - \tfrac{1}{2}(\operatorname{div} \mathbf{u}) g. \tag{87}$$

If $\mathbf{u}$ is a divergence-free velocity field, *i.e.*, $\mathbf{u} \in \mathfrak{X}_{\text{div}}$, then the ∂ and $\bar{\partial}$ derivatives of $\mathbf{u}$ reduce to:

$$\boxed{(\partial \mathbf{u})^\flat = \tfrac{1}{2}\omega} \quad \text{and} \quad \boxed{(\bar{\partial} \mathbf{u})^\flat = \mathcal{K}\mathbf{u}} \tag{88}$$

where $\omega = d(\mathbf{u}^\flat)$ is the vorticity 2-form, and $\mathcal{K}\mathbf{u}$ is the strain rate tensor of the flow.

The identities in (88) allow us to use the tools of ∂- and $\bar{\partial}$-calculus from complex differential geometry to perform calculations involving vorticity and the strain rate.

A.4 Proof of Proposition 2.2

We show that the functional gradient of the Rayleigh dissipation functional $\mathcal{R} \colon \mathfrak{X}_{\text{div}} \to \mathbb{R}$, defined by $\mathcal{R}[\mathbf{u}] = \iint_M \nu |\mathcal{K}\mathbf{u}|^2 \, dA$, is given by $(\operatorname{grad} \mathcal{R})|_{\mathbf{u}} = -2\nu \operatorname{div}(\mathcal{K}\mathbf{u})^\sharp$. Using the identity from (88), this is equivalent to showing $(\operatorname{grad} \mathcal{R})|_{\mathbf{u}} = -2\nu \star_0^{-1} d^\nabla \star_1 (\bar{\partial} \mathbf{u})$, where d^∇ denotes the covariant exterior derivative acting on vector-valued forms.

By (88), the functional $\mathcal{R}[u]$ can be written in terms of the Dolbeault operator as

$$\mathcal{R}[\mathbf{u}] = \nu \iint_M \langle \bar{\partial} \mathbf{u} \wedge \star \bar{\partial} \mathbf{u} \rangle. \tag{89}$$

Let $\mathring{\mathbf{u}} \in \mathfrak{X}_{\text{div}}$ be a divergence-free variation vanishing on ∂M. The variation of $\mathcal{R}$ in the direction $\mathring{\mathbf{u}}$ is

$$\left. \frac{d}{d\epsilon} \right|_{\epsilon=0} \mathcal{R}[\mathbf{u} + \epsilon \mathring{\mathbf{u}}] = 2\nu \iint_M \langle \bar{\partial} \mathring{\mathbf{u}} \wedge \star \bar{\partial} \mathbf{u} \rangle \tag{90}$$

$$= 2\nu \iint_M \langle \nabla \mathring{\mathbf{u}} \wedge \star \bar{\partial} \mathbf{u} \rangle, \tag{91}$$

[9] To verify that $d(\mathbf{u})^\flat [\![\mathbf{a}, \mathbf{b}]\!] = \langle \nabla_{\mathbf{a}} \mathbf{u}, \mathbf{b} \rangle - \langle \nabla_{\mathbf{b}} \mathbf{u}, \mathbf{a} \rangle$, expand the expression $d(\mathbf{u})^\flat [\![\mathbf{a}, \mathbf{b}]\!] = d_{\mathbf{a}} \langle \mathbf{u}, \mathbf{b} \rangle - d_{\mathbf{b}} \langle \mathbf{u}, \mathbf{a} \rangle - \langle \mathbf{u}, [\mathbf{a}, \mathbf{b}] \rangle$, and apply the metric compatibility property $d_{\mathbf{a}} \langle \mathbf{u}, \mathbf{b} \rangle = \langle \nabla_{\mathbf{a}} \mathbf{u}, \mathbf{b} \rangle + \langle \mathbf{u}, \nabla_{\mathbf{a}} \mathbf{b} \rangle$(similarly for the second term) along with the torsion-free property $[a, b] = \nabla_{\mathbf{a}} \mathbf{b} - \nabla_{\mathbf{b}} \mathbf{a}$.

where the second equality uses the decomposition (85) and the orthogonality of complex-linear and antilinear parts from (79). We now integrate by parts:

$$\frac{d}{d\epsilon}\Big|_{\epsilon=0} \mathcal{R}[\mathbf{u}+\epsilon\mathring{\mathbf{u}}] = -2\nu \iint_M \langle \mathring{\mathbf{u}}, d^\nabla \star \bar\partial \mathbf{u}\rangle \tag{92}$$

$$= -2\nu \iint_M \langle \mathring{\mathbf{u}}, \star_0^{-1} d^\nabla \star_1 \bar\partial \mathbf{u}\rangle \, dA \tag{93}$$

$$= \langle\!\langle \mathring{\mathbf{u}}, -2\nu \star_0^{-1} d^\nabla \star_1 \bar\partial \mathbf{u}\rangle\!\rangle. \tag{94}$$

Therefore, we conclude that $(\operatorname{grad}\mathcal{R})|_{\mathbf{u}} = -2\nu \star_0^{-1} d^\nabla \star_1 \bar\partial \mathbf{u}$. □

A.5 Proof of Proposition 3.1

We derive the natural boundary condition associated with the functional (8), which can also be expressed in the form (89). To do so, we repeat the derivation in Appendix A.4, but this time without assuming that the variation $\mathring{\mathbf{u}}$ vanishes on the boundary ∂M, thereby retaining and examining the boundary terms.

Specifically, the integration by parts in (91) now yields:

$$\frac{d}{d\epsilon}\Big|_{\epsilon=0} \mathcal{R}[\mathbf{u}+\epsilon\mathring{\mathbf{u}}] = 2\nu \oint_{\partial M} \langle \mathring{\mathbf{u}}, \star\bar\partial \mathbf{u}\rangle - 2\nu \iint_M \langle \mathring{\mathbf{u}}, d^\nabla \star \bar\partial \mathbf{u}\rangle. \tag{95}$$

Therefore, in order for the identity $(\operatorname{grad}\mathcal{R})|_{\mathbf{u}} = -2\nu \operatorname{div}(\mathcal{K}\mathbf{u})^\sharp$ to hold for all divergence-free variations $\mathring{\mathbf{u}} \in \mathfrak{X}_{\text{div}}$ that may be nonzero on ∂M, the boundary term must vanish:

$$\left\langle \mathbf{t}, (\star\bar\partial \mathbf{u})[\![\mathbf{t}]\!] \right\rangle = 0 \quad \text{on } \partial M, \tag{96}$$

where $\mathbf{t}$ denotes the unit tangent vector along the boundary curve ∂M. Using the identity (75) and setting $\mathbf{n} = J\mathbf{t}$ as the inward-pointing unit normal, condition (96) becomes:

$$-\left\langle \mathbf{t}, (\bar\partial \mathbf{u})[\![\mathbf{n}]\!] \right\rangle = 0 \quad \text{on } \partial M. \tag{97}$$

By the identity (88), this is equivalent to $(\mathcal{K}\mathbf{u})[\![\mathbf{t},\mathbf{n}]\!] = 0$. □

A.6 Proof of Theorem 2.1

Using (88), we can rewrite the Dirichlet energies from Section 2.2.1 for divergence-free vector fields $\mathbf{u} \in \mathfrak{X}_{\text{div}}$ as:

$$\mathcal{E}_{\text{D}}[\mathbf{u}] = \tfrac{1}{2} \iint_M \langle \nabla\mathbf{u} \wedge \star\nabla\mathbf{u}\rangle, \tag{98}$$

$$\mathcal{E}_{\text{H}}[\mathbf{u}] = \iint_M \langle \partial\mathbf{u} \wedge \star\partial\mathbf{u}\rangle, \tag{99}$$

$$\mathcal{E}_{\text{V}}[\mathbf{u}] = \iint_M \langle \bar\partial\mathbf{u} \wedge \star\bar\partial\mathbf{u}\rangle. \tag{100}$$

Following a similar derivation as in Appendix A.4, we find that the (negative) functional gradients of these Dirichlet energies—namely, the Bochner Laplacian (Definition 2.7), the Hodge Laplacian (Definition 2.8), and the viscous Laplacian (Definition 2.9)—can be expressed as:

$$\star_0 \Delta_{\text{B}}\mathbf{u} = d^\nabla \star_1 \nabla\mathbf{u}, \tag{101}$$

$$\star_0 \Delta_{\text{H}}\mathbf{u} = 2d^\nabla \star_1 \partial\mathbf{u} = -2Jd^\nabla\partial\mathbf{u}, \tag{102}$$

$$\star_0 \Delta_{\text{V}}\mathbf{u} = 2d^\nabla \star_1 \bar\partial\mathbf{u} = 2Jd^\nabla\bar\partial\mathbf{u}. \tag{103}$$

The second equalities in (102) and (103) follow from the complex-linear and antilinear types of $\partial\mathbf{u}$ and $\bar\partial\mathbf{u}$ (see Definition A.1 and Definition A.2), and from the identity $d^\nabla \circ J = J \circ d^\nabla$, which holds due to the metric compatibility of the Levi-Civita connection ∇.

Substituting (83) into (102) yields:

$$-2Jd^\nabla\partial\mathbf{u} = -Jd^\nabla(\nabla\mathbf{u} + J \star \nabla\mathbf{u}) \tag{104}$$

$$= -Jd^\nabla\nabla\mathbf{u} + d^\nabla \star \nabla\mathbf{u} \tag{105}$$

$$= -\star_0 K\mathbf{u} + d^\nabla \star_1 \nabla\mathbf{u}, \tag{106}$$

where we used $d^\nabla\nabla\mathbf{u} = -J\Omega^\nabla\mathbf{u}$, with $\Omega^\nabla \in \Omega^2(M)$ denoting the curvature 2-form of the connection ∇. For the Levi-Civita connection, this curvature form is the Gaussian curvature density $\star_0 K$.

Similarly, substituting (84) into (103) gives:

$$2Jd^\nabla\bar\partial\mathbf{u} = \star_0 K\mathbf{u} + d^\nabla \star_1 \nabla\mathbf{u}. \tag{107}$$

Thus, we obtain the relations:

$$\Delta_{\text{H}}\mathbf{u} = \Delta_{\text{B}}\mathbf{u} - K\mathbf{u}, \quad \Delta_{\text{V}}\mathbf{u} = \Delta_{\text{B}}\mathbf{u} + K\mathbf{u}. \tag{108}$$

□

B DERIVATION FOR THE JUMP CONDITIONS

This appendix provides the background necessary to establish Theorem 2.3, which states that the vorticity function exhibits a jump across curvature sheets.

Let $\Gamma \in M$ be an oriented curve. The *positive* (resp. *negative*) side of Γ is defined as the left (resp. right) side when traversing Γ in its oriented direction.

If a function u has a discontinuity along Γ, we denote the jump by $[u]_\Gamma : \Gamma \to \mathbb{R}$, defined as the value of u on the positive side minus its value on the negative side.

The normal vector $\mathbf{n}$ to Γ is defined by $\mathbf{n} = J\mathbf{t}$, where $\mathbf{t}$ is the unit tangent to Γ; this convention agrees with the inward unit normal when $\Gamma = \partial M$.

Let u be a function that is smooth on $M \setminus \Gamma$ but potentially discontinuous along Γ, and let φ be an arbitrary smooth test function on M. By applying Green's identity, we obtain:

$$\begin{aligned}\iint_{M\setminus\Gamma} (\Delta u)\varphi \, dA = &\int_\Gamma \left([u]_\Gamma \tfrac{\partial\varphi}{\partial\mathbf{n}} - [\tfrac{\partial u}{\partial\mathbf{n}}]_\Gamma \varphi \right) ds \\ &+ \oint_{\partial M} \left(u\tfrac{\partial\varphi}{\partial\mathbf{n}} - \tfrac{\partial u}{\partial\mathbf{n}}\varphi \right) ds + \iint_M u\Delta\varphi \, dA.\end{aligned} \tag{109}$$

Eq. (109) implies that the (weak) Laplacian of u over the entire domain M, defined via

$$\iint_M (\Delta u)\varphi \, dA \equiv \oint_{\partial M} \left(f\tfrac{\partial\varphi}{\partial\mathbf{n}} - \tfrac{\partial u}{\partial\mathbf{n}}\varphi \right) ds + \iint_M u\Delta\varphi \, dA, \tag{110}$$

can be evaluated as

$$\boxed{\iint_M (\Delta u)\varphi dA = \iint_{M\setminus\Gamma} (\Delta u)\varphi dA + \int_\Gamma \left([\tfrac{\partial u}{\partial\mathbf{n}}]_\Gamma \varphi - [u]_\Gamma \tfrac{\partial\varphi}{\partial\mathbf{n}} \right) ds.} \tag{111}$$

In other words, the Laplacian Δu can be decomposed as $\Delta u = (\Delta u)_{\text{reg}} + (\Delta u)_{\text{sing}}$, where $(\Delta u)_{\text{reg}}$ is the classical Laplacian of u away from the curve, and $(\Delta u)_{\text{sing}}$ is a distribution supported on Γ, defined by the property $\iint (\Delta u)_{\text{sing}}\varphi = \int_\Gamma ([\frac{\partial u}{\partial\mathbf{n}}]_\Gamma \varphi - [u]_\Gamma \frac{\partial\varphi}{\partial\mathbf{n}})$.

We now express this distributional singularity using Dirac-δ distributions:

Definition B.1. *Let $h : \Gamma \to \mathbb{R}$ be a function defined on Γ. The h-*weighted δ function *on Γ is the distribution $h\delta_\Gamma$ defined by*

$$\iint_M (h\delta_\Gamma)\varphi \, dA \coloneqq \int_\Gamma h\varphi \, ds, \quad \forall\, \varphi \in C^\infty(M). \tag{112}$$

The h-weighted δ' function on Γ is the distribution $h\delta'_\Gamma$ defined by

$$\iint_M (h\delta'_\Gamma)\varphi\, dA \coloneqq \int_\Gamma -h\frac{\partial\varphi}{\partial\mathbf{n}}\, ds, \quad \forall\, \varphi \in C^\infty(M). \tag{113}$$

Using the notation from Definition B.1 and eq. (109), we arrive at the following general expression for the Laplacian of a function with a jump across Γ:

$$\boxed{\Delta u = (\Delta u)_{\mathrm{reg}} + [\,\tfrac{\partial u}{\partial\mathbf{n}}]_\Gamma\delta_\Gamma + [u]_\Gamma\delta'_\Gamma.} \tag{114}$$

B.1 Proof of Theorem 2.3

We show that the vorticity equation (28) $\frac{Dw}{Dt} = \nu\Delta w + 2\nu\,\mathrm{curl}(K\mathbf{u})$ with singular Gaussian curvature $K = K_{\mathrm{reg}} + f\delta_\Gamma$ gives rise to a jump condition $[w]_\Gamma = 2f\langle\mathbf{u},\mathbf{t}\rangle$ along the curve Γ.

Note that the term $2\nu\,\mathrm{curl}(K\mathbf{u})$ is a distribution. For any test function $\varphi \in C^\infty(M)$, we have

$$\iint_M 2\nu\,\mathrm{curl}(K\mathbf{u})\varphi\, dA = \iint_M -2\nu\,\mathrm{div}(KJ\mathbf{u})\varphi\, dA \tag{115}$$
$$= 2\nu\iint_M K(J\mathbf{u})\cdot\mathrm{grad}\,\varphi\, dA \tag{116}$$
$$= 2\nu\iint_M (K_{\mathrm{reg}} + f\delta_\Gamma)(J\mathbf{u})\cdot\mathrm{grad}\,\varphi\, dA \tag{117}$$
$$= 2\nu\iint_{M\setminus\Gamma} K_{\mathrm{reg}}(J\mathbf{u})\cdot\mathrm{grad}\,\varphi\, dA + 2\nu\oint_\Gamma f\langle\mathbf{u}, -J\,\mathrm{grad}\,\varphi\rangle\, ds \tag{118}$$
$$= 2\nu\iint_M \mathrm{curl}(K_{\mathrm{reg}}\mathbf{u})\varphi\, dA + 2\nu\oint_\Gamma f\langle\mathbf{u}, -J\,\mathrm{grad}\,\varphi\rangle\, ds. \tag{119}$$

We simplify the boundary integral:

$$\oint_\Gamma f\langle\mathbf{u}, -J\,\mathrm{grad}\,\varphi\rangle\, ds = \oint_\Gamma f\langle\mathbf{u},\mathbf{t}\rangle\tfrac{\partial\varphi}{\partial\mathbf{n}}\, ds - \oint_\Gamma f\langle\mathbf{u},\mathbf{n}\rangle\tfrac{\partial\varphi}{\partial\mathbf{t}}\, ds \tag{120}$$
$$= \oint_\Gamma f\langle\mathbf{u},\mathbf{t}\rangle\tfrac{\partial\varphi}{\partial\mathbf{n}}\, ds + \oint_\Gamma \tfrac{\partial}{\partial\mathbf{t}}(f\langle\mathbf{u},\mathbf{n}\rangle)\varphi\, ds. \tag{121}$$

Thus, the singular part of $2\nu\,\mathrm{curl}(K\mathbf{u})$ is given by

$$(2\nu\,\mathrm{curl}(K\mathbf{u}))_{\mathrm{sing}} = -2\nu f\langle\mathbf{u},\mathbf{t}\rangle\delta'_\Gamma + 2\nu\tfrac{\partial}{\partial\mathbf{t}}(f\langle\mathbf{u},\mathbf{n}\rangle)\delta_\Gamma. \tag{122}$$

We now collect the regular and singular terms in the vorticity equation $\frac{Dw}{Dt} = \nu\Delta w + 2\nu\,\mathrm{curl}(K\mathbf{u})$, using the decompositions from (114) and (122):

$$\frac{Dw}{Dt} = \nu\left((\Delta w)_{\mathrm{reg}} + 2\,\mathrm{curl}(K_{\mathrm{reg}}u)\right) \tag{123}$$
$$+ \nu\left([\,\tfrac{\partial w}{\partial\mathbf{n}}]_\Gamma + 2\tfrac{\partial}{\partial\mathbf{t}}(f\langle\mathbf{u},\mathbf{n}\rangle)\right)\delta_\Gamma \tag{124}$$
$$+ \nu\left([w]_\Gamma - 2f\langle\mathbf{u},\mathbf{t}\rangle\right)\delta'_\Gamma. \tag{125}$$

For this convection-diffusion equation to admit a bounded solution w, the most singular term δ'_Γ (the weight of δ'_Γ) must vanish.[10] Hence, we conclude $[w]_\Gamma = 2f\langle\mathbf{u},\mathbf{t}\rangle$ along Γ. □

C DERIVATION FOR BOUNDARY CONDITIONS

C.1 Proof of Theorem 3.1

We show that under the natural (free-slip) boundary condition $(\mathcal{K}\mathbf{u})[\![\mathbf{t},\mathbf{n}]\!] = 0$ on ∂M, the boundary vorticity satisfies $w_\partial = 2\kappa_{\mathrm{g}}u_\partial$, where $u_\partial = \langle\mathbf{u},\mathbf{t}\rangle$ is the tangential component of the velocity along ∂M, and κ_{g} is the geodesic curvature of ∂M.

Expanding the boundary condition $(\mathcal{K}\mathbf{u})[\![\mathbf{t},\mathbf{n}]\!] = 0$ using the identity (6) gives

$$\langle\nabla_{\mathbf{t}}\mathbf{u},\mathbf{n}\rangle + \langle\nabla_{\mathbf{n}}\mathbf{u},\mathbf{t}\rangle = 0 \quad \text{on } \partial M. \tag{126}$$

[10] This can be justified rigorously by the method of dominant balance. As ϵ-mollified δ-functions tend to singular distributions, the solution behavior for $t > O(\epsilon^\alpha)$ (for some power α) becomes asymptotically governed by the equation without the most singular part, requiring the weight of δ'_Γ to vanish.

We simplify the first term:

$$\langle\nabla_{\mathbf{t}}\mathbf{u},\mathbf{n}\rangle = d_{\mathbf{t}}\cancel{\langle\mathbf{u},\mathbf{n}\rangle} - \langle\mathbf{u},\nabla_{\mathbf{t}}\mathbf{n}\rangle = \langle\mathbf{u},\mathbf{t}\rangle\kappa_{\mathrm{g}} = u_\partial\kappa_{\mathrm{g}}. \tag{127}$$

Therefore, the boundary condition becomes:

$$\langle\nabla_{\mathbf{n}}\mathbf{u},\mathbf{t}\rangle + \kappa_{\mathrm{g}}u_\partial = 0. \tag{128}$$

We now express this condition in terms of the vorticity $\omega = d\mathbf{u}^\flat = \star w$. To compute $w = \star_0^{-1}\omega$ on the boundary, we evaluate $\omega[\![\mathbf{t},\mathbf{n}]\!]$. This evaluation involves the Lie brackets of $\mathbf{t}$ and $\mathbf{n}$, so we extend both vector fields arbitrarily to a neighborhood of ∂M. Then, at the boundary:

$$w = \omega[\![\mathbf{t},\mathbf{n}]\!] = (d\mathbf{u}^\flat)[\![\mathbf{t},\mathbf{n}]\!] \tag{129}$$
$$= d_{\mathbf{t}}\cancel{\langle\mathbf{u},\mathbf{n}\rangle} - d_{\mathbf{n}}\langle\mathbf{u},\mathbf{t}\rangle - \langle\mathbf{u},[\mathbf{t},\mathbf{n}]\rangle \tag{130}$$
$$= -\langle\nabla_{\mathbf{n}}\mathbf{u},\mathbf{t}\rangle - \cancel{\langle\mathbf{u},\nabla_{\mathbf{n}}\mathbf{t}\rangle} - \langle\mathbf{u},\nabla_{\mathbf{t}}\mathbf{n} - \cancel{\nabla_{\mathbf{n}}\mathbf{t}}\rangle \tag{131}$$
$$= 2\kappa_{\mathrm{g}}u_\partial \tag{132}$$

where we have substituted (128) and applied $\langle\mathbf{u},\nabla_{\mathbf{t}}\mathbf{n}\rangle = -u_\partial\kappa_{\mathrm{g}}$. □

C.2 Proof of Theorem 3.2

We show that the friction boundary condition $2\nu(\mathcal{K}\mathbf{u})[\![\mathbf{t},\mathbf{n}]\!] = \alpha u_\partial$ implies the boundary vorticity formula $w_\partial = (2\kappa_{\mathrm{g}} - \frac{\alpha}{2\nu})u_\partial$ following the same derivation as in Appendix C.1.

Expanding the condition $2\nu(\mathcal{K}\mathbf{u})[\![\mathbf{t},\mathbf{n}]\!] = \alpha u_\partial$ yields $\langle\nabla_{\mathbf{t}}\mathbf{u},\mathbf{n}\rangle + \langle\nabla_{\mathbf{n}}\mathbf{u},\mathbf{t}\rangle - \frac{\alpha}{2\nu}u_\partial = 0$. By (127), this implies

$$\langle\nabla_{\mathbf{n}}\mathbf{u},\mathbf{t}\rangle + (\kappa_{\mathrm{g}} - \tfrac{\alpha}{2\nu})u_\partial = 0. \tag{133}$$

Now, following the computation in (129), the boundary vorticity becomes:

$$w = -\langle\nabla_{\mathbf{n}}\mathbf{u},\mathbf{t}\rangle \underbrace{- \langle\mathbf{u},\nabla_{\mathbf{t}}\mathbf{n}\rangle}_{u_\partial\kappa_{\mathrm{g}}} \overset{(133)}{=} (2\kappa_{\mathrm{g}} - \tfrac{\alpha}{2\nu})u_\partial. \tag{134}$$

□

C.3 Proof of Theorem 3.3

Here, we prove our revised form of the *Quartapelle–Valz-Gris condition*, which states that under the no-slip condition $u_\partial = 0$, the vorticity w and the harmonic coefficients $(c_1,\dots,c_m)$ must satisfy

$$\iint_M \phi_f w\, dA + \textstyle\sum_{i=1}^m c_i\oint_{\partial M} f h_{i\partial}\, ds = 0 \quad \forall\, f\colon \partial M \to \mathbb{R}, \tag{135}$$

where ϕ_f denotes the harmonic extension of f to the interior of M.

Restricting the velocity field $\mathbf{u} = -J\,\mathrm{grad}\,\psi + \sum_{i=1}^m c_i\mathbf{h}_i$ (see (31)) to the boundary and imposing the condition $u_\partial = 0$, we obtain

$$\tfrac{\partial\psi}{\partial\mathbf{n}} + \textstyle\sum_{i=1}^m c_i h_{i\partial} = 0 \tag{136}$$

where $\mathbf{n} = J\mathbf{t}$ is the inward-pointing unit normal along ∂M. Additionally, from (32), we have $-\Delta\psi = w$ in M, with Dirichlet boundary condition $\psi|_{\partial M} = 0$. Applying Green's identity gives:

$$\iint_M \phi_f w\, dA = \iint_M \phi_f(-\Delta\psi)\, dA \tag{137}$$
$$= \iint_M (-\Delta\phi_f)\psi + \oint_{\partial M}(\phi_f\tfrac{\partial\psi}{\partial\mathbf{n}} - \tfrac{\partial\phi_f}{\partial\mathbf{n}}\psi)\, ds. \tag{138}$$

Using the facts that $\Delta\phi_f = 0$, $\phi_f|_{\partial M} = f$, and $\psi|_{\partial M} = 0$, along with (136), this simplifies to $\iint_M \phi_f w\, dA = \oint_{\partial M} f(-\sum_{i=1}^m c_i h_{i\partial})\, ds$, which implies the identity in (135). □